

High Energy Neutrinos and Cosmic Rays

GÜNTER SIGL

II. Institut für theoretische Physik, Universität Hamburg, Luruper Chaussee 149, D-22761 Hamburg, Germany

Summary. — This is a summary of a series of lectures on the current experimental and theoretical status of our understanding of origin and nature of cosmic radiation. Specific focus is put on ultra-high energy cosmic radiation above $\sim 10^{17}$ eV, including secondary neutral particles and in particular neutrinos. The most important open questions are related to the mass composition and sky distributions of these particles as well as on the location and nature of their sources. High energy neutrinos at GeV energies and above from extra-terrestrial sources have not yet been detected and experimental upper limits start to put strong constraints on the sources and the acceleration mechanism of very high energy cosmic rays.

1. – Galactic and Extragalactic Primary Cosmic Radiation: A Short Overview

High energy cosmic ray (CR) particles reach from energies below 100 MeV up to at least several 10^{20} eV. One of the open questions is whether the spectrum continues to even higher energies and we just have not been able to detect it because of limited statistics or has a hard cut-off for principal physical reasons. Over the observed energy range, the differential all-particle flux drops by some 32 orders of magnitude, see Fig. 1. Cosmic rays interact in Earth's atmosphere and are thus shielded revealing their existence on the ground only by indirect effects such as ionization and the formation of showers of secondary charged particles. At energies below a few hundred GeV these

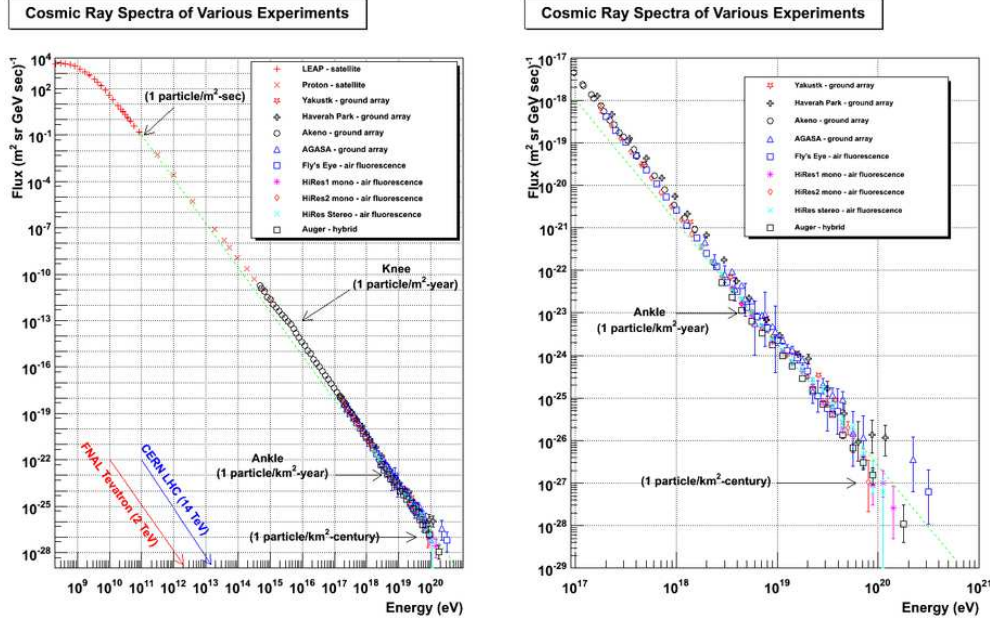


Fig. 1. – The all-particle cosmic ray spectrum and experiments relevant for its detection. The right panel is a blow-up of the highest energy region. Taken from <http://www.physics.utah.edu/~whanlon/spectrum.html>.

showers die out high above the atmosphere and are not sufficiently luminous to be visible from the ground such that they can only be detected with balloons or from satellites. Above a few hundred GeV they can be detected with telescopes from the ground and above $\sim 10^{15}$ eV, depending on the altitude of the detector, the charged secondaries and muons are sufficiently numerous to be detected on the ground. At the highest energies these air showers cover areas up to many km^2 . In 1912 Victor Hess discovered CRs by measuring ionization from a balloon [1], and in 1938 Pierre Auger proved the existence of extensive air showers (EAS) caused by primary particles with energies above 10^{15} eV by simultaneously observing the arrival of secondary particles in Geiger counters many meters apart [2].

Still, after almost 90 years of research, the origin of cosmic rays is largely an open question [3]: Only for particles of kinetic energy below 100 MeV we are sure that they have to come from the Sun the solar wind shields charged particles coming from outside the solar system at such energies. At higher energies the CR spectrum exhibits little structure and is approximated by broken power laws $\propto E^{-\gamma}$: At the energy $E \simeq 4 \times 10^{15}$ eV called the “knee”, the flux of particles per area, time, solid angle, and energy steepens from a power law index $\gamma \simeq 2.7$ to one of index $\simeq 3.0$. The bulk of the CRs up to at least that energy is believed to originate within the Milky Way Galaxy, typically by shock acceleration in supernova remnants. One of the main arguments for this comes from a

consideration of energy budgets which we will consider first.

If the CR accelerators are Galactic, they must replenish the CR flux that escapes from the Galaxy in order to sustain the observed Galactic CR differential intensity $j(E)$. Their total luminosity in CR must therefore satisfy $L_{\text{CR}} = (4\pi/c) \int dE dV t_{\text{CR}}(E)^{-1} E j(E)$, where $t_{\text{CR}}(E)$ is the mean residence time of CR with energy E in the Galaxy and V is the volume. $t_{\text{CR}}(E)$ can be estimated from the mean column density, $X(E)$, of gas in the interstellar medium that Galactic CR with energy E have traversed. Interaction of the primary CR particles with the gas in the interstellar medium leads to production of various secondary species. From the secondary to primary abundance ratios of Galactic CR it was inferred that [4]

$$(1) \quad X(E) = \rho_g t_{\text{CR}}(E) \simeq 6.9 \left(\frac{E}{20Z \text{ GeV}} \right)^{-0.6} \text{ g cm}^{-2},$$

where ρ_g is the mean density of interstellar gas and Z is the mean charge number of the CR particles. The mean energy density of CR and the total mass of gas in the Milky Way that have been inferred from the diffuse Galactic γ -ray, X-ray and radio emissions are $u_{\text{CR}} = (4\pi/c) \int dE E j(E) \simeq 1 \text{ eV cm}^{-3}$ and $M_g \sim \rho_g V \sim 4.8 \times 10^9 M_\odot$, respectively. Hence, simple integration yields

$$(2) \quad L_{\text{CR}} \sim M_g \int dE \frac{E j(E)}{X(E)} \sim 1.5 \times 10^{41} \text{ erg sec}^{-1}.$$

This is about 10% of the estimated total power output in the form of kinetic energy of the ejected material in Galactic supernovae which, from the energetics point of view, could therefore account for most of the CR. We note that the energy release from other Galactic sources, e.g. ordinary stars or isolated neutron stars [5] is expected to be too small, even for UHECR. Together with other considerations (see section 4 below) this leads to the widely held notion that CR at least up to the knee predominantly originate from first-order Fermi acceleration in supernova remnants.

Another interesting observation is that the energy density in the form of CR is comparable both to the energy density in the Galactic magnetic field ($\sim 10^{-6} \text{ G}$) as well as that in the turbulent motion of the gas,

$$(3) \quad u_{\text{CR}} \sim \frac{B^2}{8\pi} \sim \frac{1}{2} \rho_g v_t^2,$$

where ρ_g and v_t are the density and turbulent velocity of the gas, respectively. This can be expected from pressure equilibrium between the (relativistic) CR, the magnetic field, and the gas flow. If Eq. (3) roughly holds not only in the Galaxy but also throughout extragalactic space, then we would expect the extragalactic CR energy density to be considerably smaller than the Galactic one which is another argument in favor of a mostly Galactic origin of the CR observed near Earth. We note, however, that, in order for Eq. (3) to hold, typical CR diffusion time-scale over the size of the system under

consideration must be smaller than its age. This is not the case, for example, in clusters of galaxies if the bulk of CR are produced in the member galaxies or in cluster accretion shocks.

Above the knee, the all-particle CR spectrum continues with a further steepening to $\gamma \simeq 3.3$ at $E \simeq 4 \times 10^{17}$ eV, sometimes called the “second knee”. There are experimental indications that the mass composition changes from light, mostly protons, at the knee to domination by iron and even heavier nuclei at the second knee [6]. This is in fact expected in any scenario which is dominated by propagation in magnetic fields, both during acceleration and propagation from the source to the observer, and energy losses can be neglected, such that particle transport only depends on rigidity, the ratio of energy to charge, E/Z . This is usually true for baryonic Galactic cosmic rays because their interaction probability during the lifetime of the Galaxy is less than unity. Energy losses and interactions will in general break the degeneracy between E and Z because they will depend on E and Z (and possibly other quantities, such as atomic number A) separately. They become important for extra-galactic cosmic ray propagation at ultra-high energies above $\sim 10^{19}$ eV.

Above the so called “ankle” or “dip” at $E \simeq 5 \times 10^{18}$ eV, the spectrum flattens again to a power law of index $\gamma \simeq 2.8$. This is often interpreted as a cross over from a Galactic component to a harder component of extragalactic origin. The Galactic component may steepen or cut off completely because cosmic rays produced within our Galaxy are not confined by the Galactic magnetic field any more or because Galactic sources or more limited in terms of their maximal acceleration energy than extragalactic sources. However, it is also possible that the extra-galactic component already starts to dominate below the ankle, for example, around the second-knee [7] at a few times 10^{17} eV. In this case, the dip at $E \simeq 5 \times 10^{18}$ eV could also be explained as a feature induced by pair production of the extragalactic cosmic rays, provided they are predominantly protons. The observed feature is well fit for a relatively steep injection spectrum $\propto E^{-2.6-2.7}$. Below a few times 10^{17} eV diffusion in extra-galactic magnetic fields (EGMF) induces an energy dependent horizon beyond which extragalactic sources become unobservable at Earth because diffusion times become larger than the age of the Universe [8]. In addition, the effective volume-averaged injection spectrum has to flatten somewhere below $\sim 10^{18}$ eV to something not much steeper than E^{-2} , otherwise the power going into low energy cosmic rays would become prohibitive and pp interactions with the ambient gas would produce a flux of GeV–TeV γ –rays that would be higher than observed.

The proton dominance around the dip required in the low cross-over scenario can be achieved either because preferentially protons are accelerated or because extended EGMF lead to strong photo-spallation during propagation [9]. Experimental information on the mass composition above $\simeq 10^{17}$ eV is sparse [10]. The situation is particularly inconclusive around 10^{18} eV where the HiRes [11] and HiRes-MIA [12] data suggest a light (proton dominated) composition, whereas other experiments indicate a heavy composition [6]. Above $\sim 10^{17}$ eV the inferred mass composition increasingly depends on extrapolations of hadronic interaction into an energy range which cannot be measured directly because the center of mass energy of a cosmic ray of energy E with a proton

of mass m_p , $s^{1/2} \simeq (2m_p E)^{1/2} \simeq 40 (E/10^{18} \text{ eV})^{1/2} \text{ TeV}$, surpasses the maximal energy that can be attained in the laboratory. This makes them accordingly uncertain [10]. The mass composition could become lighter again above the ankle, although a significant heavy component is not excluded either.

Independently of mass composition, it is clear that cosmic rays above the ankle should have an extragalactic origin because they show no correlation with the Galactic disc. Would they have a dominantly galactic origin, they would show an anisotropy toward the galactic plane since the gyro radius of a cosmic ray of energy E and charge eZ in a magnetic field of strength B , $r_g \simeq E/(eZB) \simeq 1 (E/10^{18} \text{ eV})/Z/(B/\mu\text{G})$ becomes larger than the scale height of the Galactic disc and galactic magnetic fields can no longer isotropize the cosmic rays. Cosmic rays above 10^{18} eV are usually called ultra-high energy cosmic rays (UHECRs).

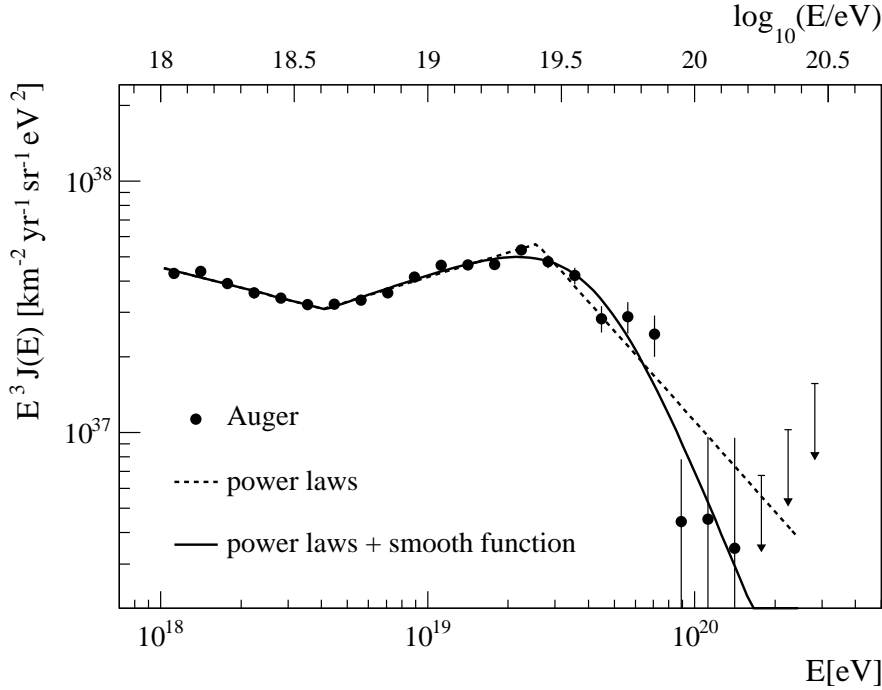


Fig. 2. – The all-particle cosmic ray spectrum measured by the Pierre Auger Observatory, from Ref. [24].

The highest energy cosmic rays in particular have challenged the imagination of physicists and astrophysicists alike. The first cosmic ray with energy above 10^{20} eV was discovered by John Linsley in 1963 at the Volcano Ranch Observatory [13]. In the 90s the famous “Fly’s Eye event” with an energy $\simeq 3 \times 10^{20} \text{ eV}$ [14] was observed and quickly scientists were starting to look for astronomical sources [15]. Around the same time, the Akeno Giant Air Shower Array (AGASA) observed an UHECR spectrum continu-

ing seemingly as a power law around 10^{20} eV. This was contrary to expectations and caused excitement because the famous Greisen-Zatsepin-Kuzmin (GZK) effect [17] predicts that nucleons loose most of their energy within about 20 Mpc above a threshold of $\simeq 6 \times 10^{19}$ eV [18] due to pion production on the cosmic microwave background (CMB). This energy loss is unavoidable because the CMB is a relic of the early Universe and is thus all-pervading. Iron nuclei have a similar reach above $\simeq 6 \times 10^{19}$ eV and intermediate mass nuclei have an even smaller horizon [19, 20]. This implies that above this so-called GZK threshold only sources within $\simeq 50$ Mpc should be visible. As long as there is no strong over-density of UHECR sources within that distance scale, this would predict a strong suppression of the UHECR flux above the GZK threshold. This is often, somewhat misleadingly, called the “GZK cutoff”. It is, however, not a strict cut-off because sources within $\simeq 50$ Mpc are still visible up to much higher energies. Meanwhile, a flux suppression consistent with the GZK effect has been observed by the more recent High Resolution Fly’s Eye [21, 22] and Pierre Auger [23, 24, 25] experiments, see Fig. 2. It is likely that the seeming absence of the GZK suppression in the AGASA spectrum was due energy calibration problems.

Excellent recent and more in-depth reviews on galactic and extragalactic cosmic rays can be found in Ref. [26] and [27], respectively.

2. – Cosmic Ray Acceleration

2.1. Shock Acceleration. – In 1949 Enrico Fermi observed that when a charged particles collides against moving magnetic fields, for example magnetized interstellar clouds moving in random directions with a velocity v within our Galaxy, on average there is an average fractional energy gain per collision of order v^2 [28]. This is because although the particle gains energy when moving towards the “magnetic mirror” and loses when moving away from it, on average the probability for approaching the mirror is higher than the one for receding from the mirror. Nowadays this is called “second order Fermi acceleration”. However, if the “magnetic mirror” is regularly shaped, for example, as a plain wave as is the case at a magnetized shock front, the fractional energy gain per reflection turns out to be first order in the velocity v of the moving mirror, which strongly increases the acceleration efficiency for non-relativistic motion. This case today is known as “first order Fermi acceleration” and below we will focus on this case which we will discuss in detail.

We start with a few general considerations. The force of an electromagnetic field \mathbf{E}, \mathbf{B} on a particle of charge eZ and velocity $\boldsymbol{\beta}$ is given by

$$(4) \quad \mathbf{F} = eZ (\mathbf{E} + \boldsymbol{\beta} \times \mathbf{B}) .$$

Consider a particle of momentum \mathbf{p} and energy E gyrating with an angular frequency ω_g in a homogeneous magnetic field \mathbf{B}_0 . It will experience a force $\omega_g \mathbf{p} = eZ(\mathbf{p} \times \mathbf{B}_0)/E$,

resulting in

$$(5) \quad \omega_g = \frac{eZB_{\perp}}{E},$$

where $B_{\perp} = |\mathbf{p} \times \mathbf{B}_0|/p$ is the modulus of the component of \mathbf{B}_0 perpendicular to the motion of the charge. The gyro-radius, which is also called Larmor radius, is given by

$$(6) \quad r_g(p) = \frac{\beta}{\omega_g} = \frac{p/E}{\omega_g} = \frac{p}{eZB_{\perp}}.$$

Note that the equation of motion only depends on rigidity, p/Z .

Astrophysical plasmas are often highly conducting, thus when the plasma flow velocity is \mathbf{v} , we have $\mathbf{E} \simeq -\mathbf{v} \times \mathbf{B}$, and thus $\mathbf{E} = 0$ in the plasma rest frame.

Charged particles with a gyro-radius Eq. (6) much smaller than the size of the magnetized region are diffusing in the magnetic field. In a general diffusion process a particle with a mean scattering length λ over which it changes direction will propagate an average squared distance $\langle d^2 \rangle \sim \lambda t$ over time t . The in general energy dependent scattering length $\lambda(p)$ is often called the diffusion coefficient $D(p)$. In case of diffusion in magnetic fields, charged particles typically scatter on inhomogeneities of the magnetic field and energy loss due to collisions with ambient gas or low energy photons is often negligible, except at the highest energies. In this case the diffusion coefficient $D(p)$ will depend on the detailed structure of the magnetic field, but will typically be larger than or comparable to the gyro-radius Eq. (6),

$$(7) \quad D(p) \gtrsim \frac{1}{3} r_g(p).$$

The lower limit is often called the *Bohm limit*.

A shock is basically a solution of the hydrodynamics equations with a discontinuity in the flow of a fluid or plasma. We will here only consider plane shocks. In the "shock frame" in which the shock is at rest, the plasma is moving toward the shock with a velocity u_1 from the "upstream" side, and moving away from the shock on the opposite, "downstream" side with a velocity $u_2 < u_1$. The situation is depicted in Fig. 3 where we define the positive z -direction as perpendicular to the shock front pointing toward the downstream region. In the Fermi acceleration process, cosmic rays cross back and forth across astrophysical shocks by scattering on inhomogeneities of the magnetic fields. As we will show in the following, in each shock crossing, on average they gain energy, but also have a finite probability for escaping the acceleration region. This interplay between energy gain and particle loss will lead to a power law spectrum. We consider here only the simplest case where the magnetic field is fully turbulent without any coherent component and we restrict ourselves to the *test particle regime* in which the back-reaction of accelerated CRs on the shock properties is neglected. For a comprehensive review of shock acceleration theory see Ref. [29].

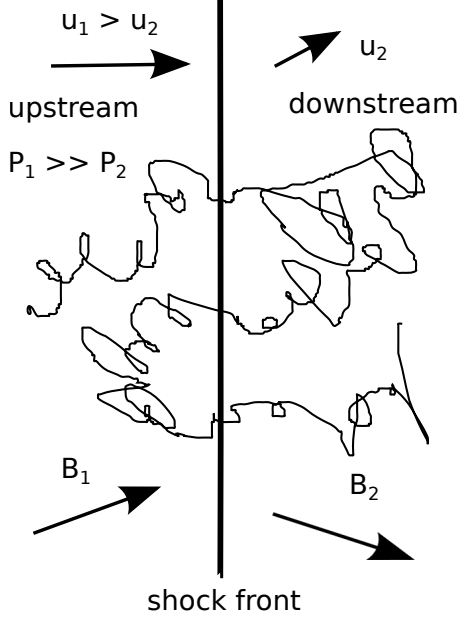


Fig. 3. – For a plane, adiabatic shock the jumps in mass density, velocity, and pressure are given by the Rankine-Hugoniot conditions and determine the compression ratio $r \equiv \rho_2/\rho_1$. Upstream and downstream regions are denoted with index 1 and 2, respectively.

Let us now consider one cycle of shock crossing of ultra-relativistic particles, $p \simeq E$, $\beta \simeq 1$, for a non-relativistic shock. In the plasma rest frame where $\mathbf{E} = 0$, the particle momentum is constant. Let us denote the angle of its direction of motion relative to the z -direction with θ_i , and $\mu_i \equiv \cos \theta_i$, for $i = 1, 2$. A relativistic particle of momentum p_1 in the upstream rest frame approaching the shock front has $\mu_1 > -u_1$ and will have a momentum $p_2 = \Gamma p_1 (1 + v\mu_1)$ in the downstream rest frame, where $v = (u_1 - u_2)/(1 - u_1 u_2)$ with corresponding Lorentz factor $\Gamma = (1 - v^2)^{-1/2}$. Similarly, a particle with momentum p_2 in the downstream rest frame approaching the shock has $\mu_2 < -u_2$ and will have a momentum $p_1 = \Gamma p_2 (1 - v\mu_2)$ in the upstream rest frame. After one cycle we thus have

$$(8) \quad p'_1 = \Gamma^2 p_1 (1 - v\mu_2)(1 + v\mu_1).$$

Assuming an isotropic distribution in both plasma rest frames and averaging the fluxes $\propto \mu_i$ over the shock front over $-u_1 \leq \mu_1 \leq 1$ and $-1 \leq \mu_2 \leq -u_2$, for non-relativistic shocks, $u_1, u_2, v \ll 1$ leads to an average momentum gain of

$$(9) \quad \langle \Delta p \rangle \simeq \frac{4}{3} (u_1 - u_2) p$$

during one cycle, where p is the initial momentum. If there is no shock, then $u_1 - u_2$ and

there is no acceleration as it should be because in this case there is only one reference frame and thus no electric field in its rest frame that could change the energy of the particles.

We can estimate the downstream escape probability as the ratio of the convective flux far from the shock front to the flux entering the downstream region from the upstream region. Assuming a constant cosmic ray mass density n downstream, one has

$$(10) \quad P_{\text{esc}} \simeq \frac{nu_2}{\frac{n}{4\pi} 2\pi \int_0^1 d\mu_2 \mu_2} = 4u_2.$$

We can now estimate the spectrum as follows: Starting with a momentum p_0 , after n cycles, the cosmic rays that have not escaped the downstream region yet will on average have momentum $p_n \simeq p_0 (1 + \langle \Delta p \rangle / p)^n$, and a density of $n(> p_n) = n(> p_0)(1 - P_{\text{esc}})^n$. Writing the integral spectrum of such cosmic rays as $n(> p_n) = n(> p_0)(p_n/p_0)^{1-\alpha}$, taking the logarithm yields

$$(11) \quad \alpha = 1 - \frac{\ln [n(> p_n)/n(> p_0)]}{\ln (p_n/p_0)} = \frac{r+2}{r-1},$$

where $r \equiv u_1/u_2 = \rho_2/\rho_1 > 1$ is the shock compression ratio because mass conservation implies $\rho_1 u_1 = \rho_2 u_2$, where $\rho_{1,2}$ are the energy densities on the two sides of the shock. The second equality holds for non-relativistic shocks.

Let us now compute the compression ratio r in terms of the properties of the plasma. The flow of plasma across the shock front conserves mass, momentum and energy,

$$(12) \quad \begin{aligned} \rho_1 u_1 &= \rho_2 u_2, \\ \rho_1 u_1^2 + P_1 &= \rho_2 u_2^2 + P_2, \\ \rho_1 u_1 \left(\frac{1}{2} u_1^2 + h_1 \right) &= \rho_2 u_2 \left(\frac{1}{2} u_2^2 + h_2 \right), \end{aligned}$$

where P_i and h_i are pressure and specific enthalpy, respectively, of the plasma on the two sides, $i = 1, 2$. The specific enthalpy is the "available" energy of a system under constant pressure. It is given by $h = (\rho_{\text{kin}} + P)/\rho$, where ρ_{kin} is the kinetic (excluding rest mass) energy density. For an ideal, non-relativistic gas $P \propto \rho$ and thus the speed of sound $c_s^2 = dP/d\rho = P/\rho$. Furthermore, $P/\rho_{\text{kin}} = \gamma - 1$, where γ is the adiabatic index. For an ideal, non-relativistic gas it is $\gamma = 5/3$, so that one has $P = \frac{2}{3}\rho_{\text{kin}} = nT = \frac{\rho}{m}T$, where m and T are mass and temperature of the particles and we have used $\rho_{\text{kin}} = \frac{1}{2}nm\langle v^2 \rangle = \frac{3}{2}nT$ with $\langle v^2 \rangle$ the average squared particle velocity at temperature T . Thus, in this case $c_s^2 = T/m$. In general, one thus has $h = \frac{\gamma}{\gamma-1}c_s^2 = \frac{\gamma}{\gamma-1}P/\rho$.

Eqs. (12) are often called the Rankine-Hugoniot jump conditions. Dividing the last one by $\rho_1 u_1 u_2^2 = \rho_2 u_2^3 = \rho_1 u_1^3 / r^2$ [these equalities are a consequence of the first condition in Eqs. (12)], we obtain

$$(13) \quad r^2 \left(\frac{1}{2} + \frac{\gamma}{\gamma-1} \frac{1}{\mathcal{M}^2} \right) = \frac{1}{2} + \frac{\gamma}{\gamma-1} \frac{P_2}{\rho_2 u_2^2} = \frac{1}{2} + \frac{\gamma}{\gamma-1} r \frac{P_2}{\rho_1 u_1^2},$$

where we have introduced the upstream Mach number $\mathcal{M} \equiv u_1/c_{s,1}$. Using the second condition in Eqs. (12), we can express P_2 in terms of upstream quantities, $P_2 = P_1 + \frac{r-1}{r}\rho_1 u_1^2$. With this, the right hand side of Eq. (13) becomes $-(\gamma + 1)/[2(\gamma - 1)] + \gamma(1 + \mathcal{M}^{-2})r/(\gamma - 1)$. This yields a quadratic equation for r whose largest solution is

$$(14) \quad r = \frac{\gamma + 1}{\gamma - 1 + 2\gamma/\mathcal{M}^2}.$$

We now realize that for non-relativistic shocks with $\gamma = 5/3$ we have $r \leq 4$ and from Eq. (11) $\alpha \geq 2$, where the limiting values are obtained in the limit of large Mach number, $\mathcal{M} \gg 1$.

We can estimate the time scales associated with acceleration as follows: In the limit of an infinitely extended shock the escape time is given by equating the downstream convection and diffusion distances, $u_2 T_{\text{esc}} \simeq [2D_2(p)T_{\text{esc}}]^{1/2}$, with $D_2(p)$ the downstream diffusion coefficient, or

$$(15) \quad T_{\text{esc}}(p) \simeq \frac{2D_2(p)}{u_2^2}$$

Furthermore, the cycle time scale is $T_{\text{cyc}} \simeq P_{\text{esc}} T_{\text{esc}}$ and the acceleration time scale is $T_{\text{acc}} \simeq (p/\langle \Delta p \rangle) T_{\text{cyc}}$, giving

$$(16) \quad \begin{aligned} T_{\text{cyc}}(p) &\simeq \frac{D_2(p)}{2u_2} \\ T_{\text{acc}}(p) &\simeq \frac{3D_2(p)}{8(u_1 - u_2)u_2}, \end{aligned}$$

where we have used Eqs. (10) and (9). In cases where collisional energy losses can not be neglected, one can obtain the maximal energy by comparing $T_{\text{acc}}(p)$ to the relevant energy loss time scales, such as inverse Compton scattering (ICS), synchrotron radiation, pion production, to be discussed below, as well as with the shock lifetime.

Relativistic shocks with $u_1, v \rightarrow 1$ are more complicated to treat because the particle distributions can not be assumed isotropic anymore. Nevertheless, in the most optimistic scenarios, one has

$$(17) \quad T_{\text{acc}}(p) \sim D(p) \sim r_g(p) \sim \frac{p}{eZB}.$$

It is obvious from Eq. (8) that as long as particles are isotropically distributed in the intervals $-u_1 \leq \mu_1 \leq 1$ and $-1 \leq \mu_2 \leq -u_2$, one has $\langle p'_1 \rangle \sim 2\Gamma^2 p_1$ for relativistic shocks and thus particles gain energy very efficiently in one cycle. However, in a highly relativistic shock, the upstream plasma frame approaches the shock with almost the speed of light, $u_1 \simeq 1$, and thus, after returning from the downstream frame at the end of the first cycle, the CR may not have sufficient time to isotropize before being caught up by the shock. In this case, the projection of the CR velocity onto the shock normal

μ_1 is given by the same quantity on the downstream region by a Lorentz transformations as $\mu_1 \equiv p_{1,z}/p_1 = (p_{2,z} - vp_2)/[p_2(1 - v\mu_2)] = (\mu_2 - v)/(1 - v\mu_2)$. Therefore, the factor $(1 + v\mu_1)$ in Eq. (8) becomes $1/[\Gamma^2(1 - v\mu_2)] \sim 1/(2\Gamma^2)$ since the condition for crossing from downstream to upstream requires $\mu_2 \simeq -1$ for a relativistic shock for which also $u_2 \simeq 1$. Using Eq. (8) again then yields $\langle p'_1 \rangle \simeq p_1$ and thus there is little energy gain after the first cycle.

2.2. Maximal Acceleration Energy. – Let us now estimate the maximal energy up to which cosmic rays can be accelerated in shocks. In this section we consider all quantities in the shock rest frame. If the shock itself moves with a Lorentz factor Γ , there will be a geometry-dependent relation between quantities in the shock rest frame and in the observer frame. As an example for this case we will consider the fireball model for gamma-ray bursts in more detail in the next section.

At very high energies, Eq. (15) becomes larger than the diffusion time over the finite linear size R of the shock,

$$(18) \quad T_{\text{esc}}^R \simeq \frac{R^2}{D(p)} \gtrsim \frac{R^2}{r_g(p)} \simeq \frac{eZB_{\text{rms}}R^2}{p},$$

where we have used Eq. (7). Since acceleration requires $T_{\text{acc}} \lesssim T_{\text{esc}}^R$, using Eq. (16) for the acceleration time scale with $D(p) \gtrsim r_g(p)$, this results in the famous Hillas criterion [30],

$$(19) \quad E_{\text{max}} \lesssim eZRBv \simeq 10^{18} v \left(\frac{B}{\mu\text{G}} \right) \left(\frac{R}{\text{kpc}} \right) \text{ eV},$$

where we have abbreviated the root mean square of the magnetic field B_{rms} by B . There is another, quicker and more qualitative derivation of Eq. (19) that also gives an order of magnitude estimate of the acceleration time scale Eq. (16): The time scale at which diffusion and convection length scales become comparable in the shock, $d \sim D(p)t \sim (vt)^2$, is given by $t \sim D(p)/v^2$. Requiring that the corresponding length scale d is smaller than the shock size, $d \simeq D(p)/v \lesssim R$ immediately results in Eq. (19) when Eq. (7), $D(p) \gtrsim r_g(p)$, with the gyro radius $r_g(p)$ given by Eq. (6) is used.

Note that for relativistic shocks, $v \simeq 1$, the Hillas criterion is equivalent to the intuitive condition that the gyro radius has to be smaller than the size of the shock, $r_g(p) \lesssim R$. The Hillas criterion is shown and compared with various astrophysical objects in Fig. 4.

Accelerating particles of charge eZ to an energy E_{max} also requires a minimal source power which can be estimated as follows: Acceleration to an energy E_{max} requires an induction $\mathcal{E} \gtrsim E_{\text{max}}/(eZ)$. With $Z_0 \simeq 100\Omega$ the vacuum impedance, this leads to the dissipation of a minimal power of [31, 32]

$$(20) \quad L_{\text{min}} \simeq \frac{\mathcal{E}^2}{Z_0} \simeq 10^{45} Z^{-2} \left(\frac{E_{\text{max}}}{10^{20} \text{ eV}} \right)^2 \text{ erg s}^{-1}.$$

When expressing the square of the product of the magnetic field in an accelerator with its size in terms of a luminosity, $L \sim B^2 R^2$, this condition can be expressed in terms of the

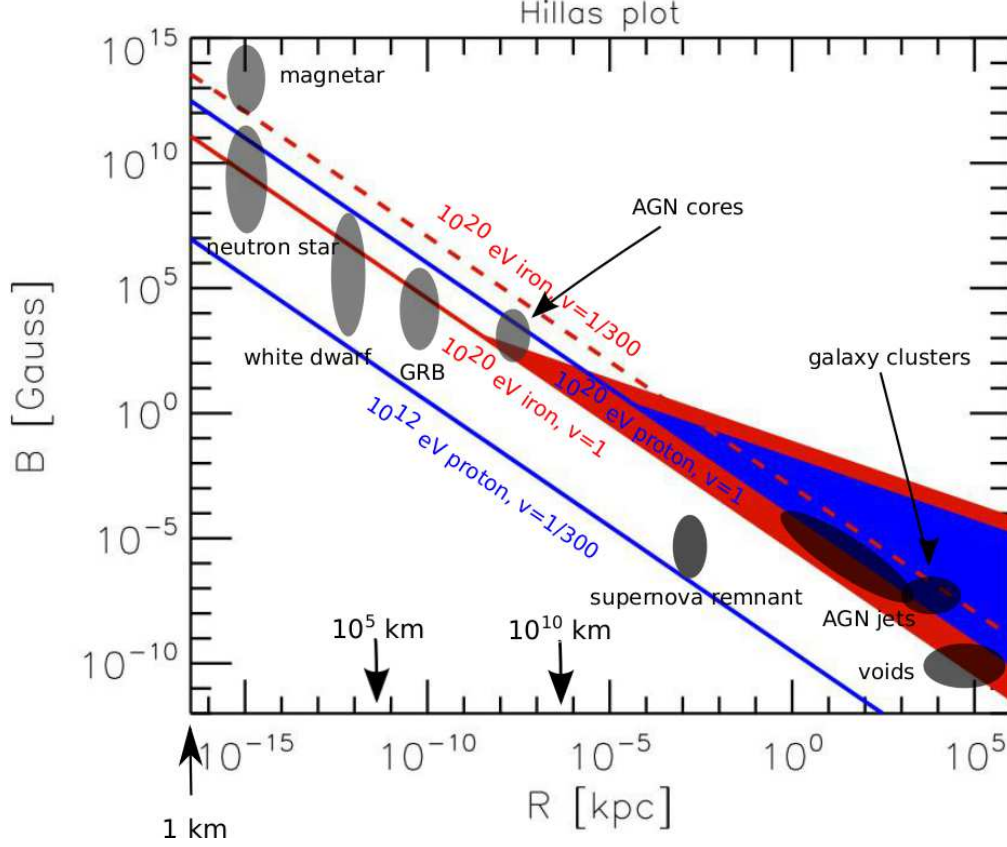


Fig. 4. – The “Hillas plot” represents astrophysical objects which are potential cosmic-ray accelerators on a two-dimensional diagram where on the horizontal direction the size linear extension R of the accelerator, and on the vertical direction the magnetic field strength B are plotted. According to Eq. (19), the maximal acceleration energy E is proportional to $ZRBv$, where v is the shock velocity in units of the speed of light and Z is the particle charge. Particular values for the maximal energy correspond to diagonal lines in this diagram and can be realized either in a large, low field acceleration region or in a compact accelerator with high magnetic fields. For a shock velocity $v \sim 1$, neutron stars, AGN, Radio Galaxies or Galactic clusters can accelerate protons to $E \sim 10^{20}$ eV. For typical non-relativistic shocks, $v \sim 1/300$, as they are realized, for example, in supernova remnants, no astrophysical objects of sufficient size and magnetic field to produce 10^{20} eV protons are known. The blue and red shaded wedges signify the parameter ranges satisfying both the Hillas condition Eq. (19) and the synchrotron condition Eq. (22) for a 10^{20} eV proton and iron, respectively in the shock rest frame

Hillas-criterium Eq. (19) for relativistic shocks, $v \simeq 1$, which states that the gyro radius of a charged particle at the maximal acceleration energy must fit within the accelerator of size R . Eq. (20) suggests that the power requirements are considerably relaxed for heavier nuclei which is easy to understand because an estimate solely based on motion

of charged particles in magnetic fields can only depend on their rigidity E/Z .

However, the Hillas criterion Eq. (19) and the minimal power Eq. (20) are necessary but in general not sufficient since they do not take into account energy loss processes within the source. If the approximation of collision-less acceleration is not good, the maximal energy is further constrained by the condition that the acceleration time scale must not only be smaller than the escape time, but also smaller than the energy loss time over which the particle loses a given fraction of its energy. The most important energy loss processes for cosmic rays will be discussed in section 4 below. Furthermore, the shock may only have a finite lifetime T_{dyn} which gives an additional condition. The most general version of the equation determining the maximal energy is thus

$$(21) \quad T_{\text{acc}}(p) \lesssim \min [T_{\text{esc}}^L(p), T_{\text{loss}}(p), T_{\text{dyn}}] .$$

The modifications resulting from taking into account energy loss processes have recently been discussed in Ref. [33]. For example, for diffuse shock acceleration synchrotron radiation by the accelerated nuclei is the dominant energy loss mechanism and yields the additional constraint

$$(22) \quad E_{\text{max}} \lesssim 3 \times 10^{16} \frac{A^4}{Z^4} \left(\frac{B}{\text{G}} \right)^{-2} \left(\frac{R}{\text{kpc}} \right)^{-1} \text{ eV} .$$

This equation essentially follows from integrating the synchrotron energy loss rate

$$(23) \quad \left. \frac{dE}{dt} \right|_{\text{syn}} \simeq - \frac{e^4}{36\pi^2 m_p^4} \left(\frac{Z}{A} \right)^4 B^2 E^2$$

over the length scale R [34], where m_p is the proton mass. The additional constraint Eq. (22) is shown for 10^{20} eV protons and iron nuclei as the colored wedges in Fig. 4.

Acceleration is often assumed to be rigidity limited such that the differential flux of nuclei of charge Z at energy E can, for example, be assumed to be of power-law form

$$(24) \quad \Phi_{Z,A}(E) = \frac{dN_{Z,A}}{dE} \propto q_{Z,A} E^{-\alpha} \Theta(Z E_{\text{max,p}} - E) ,$$

where $q_{Z,A}$ is the relative abundance of the nucleus of charge Z and atomic number A at a given energy E , α is the differential spectral index, $E_{\text{max,p}}$ is the maximal proton energy and $\Theta(x)$ is the Theta-function which cuts off the spectrum for $E > Z E_{\text{max,p}}$. To compare with abundances in a non-relativistic gas, one often refers to abundances $x_{Z,A}$ at a given energy per nucleon E/A , such that for a differential spectrum with power-law index s one has

$$(25) \quad q_{Z,A} \propto x_{A,Z} A^{\alpha-1} .$$

Thus, a steep spectrum can lead to a strong enhancement of the abundance of heavy nuclei compared to the abundances in the gas at rest.

2.3. Application to Particle Acceleration in Gamma-Ray Bursts. – In the following we will apply the conditions for the maximal energy to a particular potential UHECR source class, namely gamma-ray bursts (GRBs) [35, 36]. In the fireball model of GRBs an optically thick plasma of photons, leptons and baryons expands until it becomes transparent to the γ -rays. During the ensuing so called “prompt phase” the fireball expands with a Lorentz factor $\Gamma \gg 1$ which depends on its baryon content. Since different parts of the fireball will move with slightly different velocities, different shells will form which will crash into each other and form shocks at which first order Fermi acceleration can take place. Finally, when crashing into the extragalactic medium the fireball will also form external shocks which would explain the GRB afterglow. The formation of internal shocks explains the variability on time scales $t_v \sim 0.01$ s observed during the prompt phase. Since the individual shells approach the observer with velocities $v \sim 1 - 1/(2\Gamma^2)$, the typical radius of an internal shock in the observer frame will be $r_i \simeq t_v/(1 - v) \simeq 2\Gamma^2 t_v$. Note that this relation is purely kinematic and not a relativistic effect because all quantities correspond to the same observer frame. In the following quantities measured in the comoving rest frame of the internal shocks will be denoted by a prime and we will in part follow the notations in Ref. [37]. We assume that a fraction ϵ_e of the turbulent kinetic energy density u'_{kin} carried by the baryons, will be converted into electrons and positrons and a similar part to γ -rays. The photon energy density in the shock rest frame is, therefore, given by $u'_\gamma \simeq \epsilon_e u'_{\text{kin}}$. Photon energies in the observer and the shock rest frame are related by $\varepsilon = \Gamma \varepsilon'$. Since a length interval Δx measured at equal time in the observer frame, $\Delta t = 0$, transforms as $\Delta x = \Delta x'/\Gamma$, the average photon number density per volume and energy $n_\gamma(\varepsilon)$ and $n'_\gamma(\varepsilon')$ is invariant under Lorentz transformation and thus one has $n'_\gamma(\varepsilon') = n_\gamma(\Gamma \varepsilon')$. This implies $u'_\gamma = \int d\varepsilon' \varepsilon' n'_\gamma(\varepsilon') = \int d\varepsilon \varepsilon n_\gamma(\varepsilon)/\Gamma^2 \sim L_\gamma/(4\pi\Gamma^2 r_i^2)$, where L_γ is the GRB luminosity in the observer rest frame. For the magnetic energy density in the shock rest frame u'_B we assume $u'_B = (B')^2/(8\pi) \simeq \epsilon_B u'_{\text{kin}}$. Observations indicate $\epsilon_B \simeq \epsilon_e \simeq 0.1$. After elimination of u'_{kin} , one can estimate the magnetic field in the shock rest frame as

$$(2\mathfrak{B}') \simeq \left(\frac{\epsilon_e}{\epsilon_B}\right)^{1/2} \frac{L_\gamma/2}{\Gamma^3 t_v} \simeq 5 \times 10^4 \left(\frac{\epsilon_e}{\epsilon_B}\right)^{1/2} \left(\frac{L_\gamma}{10^{52} \text{ erg s}^{-1}}\right)^{1/2} \left(\frac{300}{\Gamma}\right)^3 \left(\frac{0.01 \text{ s}}{t_v}\right) \text{ G}.$$

This also allows to understand the rough structure of the GRB γ -ray spectrum: In the shock frame the characteristic energy of the electrons and positrons will be of the order $\epsilon_e m_p$. These electrons and positrons will emit synchrotron photons in the magnetic field Eq. (26) with a characteristic energy in the observer frame of

$$(27) \varepsilon_0 \simeq \Gamma \frac{3eB'}{2m_e^3} (\epsilon_e m_p)^2 \simeq 0.88 \epsilon_e^{3/2} \epsilon_B^{1/2} \left(\frac{L_\gamma}{10^{52} \text{ erg s}^{-1}}\right)^{1/2} \left(\frac{300}{\Gamma}\right)^3 \left(\frac{0.01 \text{ s}}{t_v}\right) \text{ MeV},$$

with m_e the electron mass. The observed γ -ray spectrum $n_\gamma(\varepsilon)$ of GRBs can be approximated by a broken power law with an index $-\alpha \simeq -1$ for $\varepsilon \lesssim \varepsilon_0$ and index $-\beta \simeq -2.2$ for $\varepsilon \gtrsim \varepsilon_0$, where the observed break energy $\varepsilon_0 \sim 1$ MeV, consistent with Eq. (27).

The acceleration time scale in the shock frame Eq. (17) for relativistic shocks then becomes

$$\begin{aligned}
 T'_{\text{acc}}(E) &\sim \frac{\eta E'}{e B'} \sim \left(\frac{2\epsilon_e}{\epsilon_B L_\gamma} \right)^{1/2} \frac{\eta \Gamma^2 E t_v}{e} \\
 (28) \quad &\simeq 6.6 \times 10^{10} \left(\frac{\epsilon_e}{\epsilon_B} \right)^{1/2} \left(\frac{10^{52} \text{ erg s}^{-1}}{L_\gamma} \right)^{1/2} \eta \left(\frac{\Gamma}{300} \right)^2 \left(\frac{E}{300 \text{ EeV}} \right) \left(\frac{t_v}{0.01 \text{ s}} \right) \text{ cm}.
 \end{aligned}$$

We have put $Z = 1$ here because nuclei are quickly photo-disintegrated in GRBs [89].

One condition on the maximal acceleration energy is now obtained by comparing Eq. (28) with the dynamical and energy loss times scales, according to the condition Eq. (21). The dynamical times scale in the shock frame where $\Delta x'$ is given by

$$(29) \quad T'_{\text{dyn}} \simeq \frac{r_i}{\Gamma} \simeq 2\Gamma t_v \simeq 1.8 \times 10^{11} \left(\frac{\Gamma}{300} \right) \left(\frac{t_v}{0.01 \text{ s}} \right) \text{ cm},$$

which, together with the characteristic magnetic field strength in the shock rest frame Eq. (26) is also marked “GRB” in Fig. 4. Note that because of relativistic boosting, the energy which has to be reached in the shock rest frame is smaller than the observed energy E by a factor Γ . Altogether,

$$(30) \quad E_{\text{max}} \lesssim 8.2 \times 10^{20} \left(\frac{\epsilon_B}{\epsilon_e} \right)^{1/2} \left(\frac{L_\gamma}{10^{52} \text{ erg s}^{-1}} \right)^{1/2} \left(\frac{1}{\eta} \right) \left(\frac{300}{\Gamma} \right) \text{ eV},$$

which is independent of t_v . In fact, this is a generalization of Eq. (20) to which it reduces for $\Gamma = 1$. We now consider the constraint on the maximal energy from synchrotron radiation by the protons. The synchrotron cooling time scale is

$$\begin{aligned}
 T'_{\text{synch}}(E) &\sim \frac{(6\pi)^2 m^4}{e^4 E' (B')^2} = \frac{2(6\pi)^2 m^4}{e^4} \left(\frac{\epsilon_e}{\epsilon_B L_\gamma} \right) \frac{\Gamma^7 t_v^2}{E} \\
 (31) \quad &\simeq 8.4 \times 10^{12} \left(\frac{\epsilon_e}{\epsilon_B} \right) \left(\frac{10^{52} \text{ erg s}^{-1}}{L_\gamma} \right) \left(\frac{\Gamma}{300} \right)^7 \left(\frac{300 \text{ EeV}}{E} \right) \left(\frac{t_v}{0.01 \text{ s}} \right)^2 \text{ cm}.
 \end{aligned}$$

Comparing this with Eq. (28) leads to

$$(32) \quad E_{\text{max}} \lesssim 3.4 \times 10^{21} \left(\frac{\epsilon_e}{\epsilon_B} \right)^{1/4} \left(\frac{10^{52} \text{ erg s}^{-1}}{L_\gamma} \right)^{1/4} \frac{1}{\eta^{1/2}} \left(\frac{\Gamma}{300} \right)^{5/2} \left(\frac{t_v}{0.01 \text{ s}} \right)^{1/2} \text{ eV}.$$

Finally, we estimate photo-hadronic energy loss rates, namely pion production of the accelerated protons on the radiation field within the GRB, $p\gamma \rightarrow N\pi$. In the shock frame pion production of a proton of energy E' can only occur with photons of energy $\varepsilon' \gtrsim \varepsilon'_{N\pi} \sim m_\pi m_p / (2E')$, with m_π the pion mass, as can be seen from Eq. (46) below. Far above the threshold the cross section can be approximated by $\sigma_{N\pi} \simeq 150 \mu\text{b}$ and the

protons loose a substantial fraction of their energy in each interaction. Therefore, the pion production loss time can be estimated from

$$(33) \quad \frac{1}{T'_{N\pi}(E')} \sim \sigma_{N\pi} \varepsilon'_{N\pi} n'_\gamma(\varepsilon'_{N\pi}) \simeq \frac{\sigma_{N\pi} m_\pi m_p}{2E'} n_\gamma \left(\frac{\Gamma m_\pi m_p}{2E'} \right).$$

Since $n_\gamma(\varepsilon) \propto \varepsilon^{-1}$ for $\varepsilon \lesssim \varepsilon_0$, one has $\varepsilon n_\gamma(\varepsilon) \sim L_\gamma / (4\pi \varepsilon_0 r_i^2)$ for $\varepsilon \lesssim \varepsilon_0$. Therefore, the interaction rate Eq. (33) is roughly energy independent above the energy

$$(34) \quad E_{p\pi} \simeq \frac{\Gamma^2 m_\pi m_p}{2\varepsilon_0} \simeq 4 \times 10^{16} \left(\frac{\Gamma}{300} \right)^2 \left(\frac{\text{MeV}}{\varepsilon_0} \right) \text{ eV}$$

and corresponds to an energy loss time of

$$(35) \quad \begin{aligned} T'_{N\pi}(E > E_{p\pi}) &\sim \frac{16\pi \varepsilon_0 \Gamma^5 t_v^2}{\sigma_{N\pi} L_\gamma} \\ &\simeq 3.5 \times 10^{11} \left(\frac{\varepsilon_0}{\text{MeV}} \right) \left(\frac{10^{52} \text{ erg s}^{-1}}{L_\gamma} \right) \left(\frac{\Gamma}{300} \right)^5 \left(\frac{t_v}{0.01 \text{ s}} \right)^2 \text{ cm}. \end{aligned}$$

Comparing this with Eq. (28) finally gives the additional condition

$$(36) \quad E_{\text{max}} \lesssim 1.6 \times 10^{21} \left(\frac{\varepsilon_0}{\text{MeV}} \right) \left(\frac{\epsilon_B}{\epsilon_e} \right)^{1/2} \left(\frac{10^{52} \text{ erg s}^{-1}}{L_\gamma} \right)^{1/2} \frac{1}{\eta} \left(\frac{\Gamma}{300} \right)^3 \left(\frac{t_v}{0.01 \text{ s}} \right) \text{ eV}.$$

Although GRBs individually have more than adequate power to achieve the required maximal acceleration energies, they are disfavored in terms of the local power density they can provide in the form of UHECRs [39] compared to an UHECR origin in AGNs and radio galaxies.

3. – Anisotropies and Nature of the Sources

Although the main goal of the IceCube experiment [40] originally was the detection of extraterrestrial high energy neutrinos via up-going muons, it is also an excellent detector of galactic CRs via the down going muon tracks (see section 6 below) that are produced by the interactions of cosmic rays in the Earth's atmosphere. By May 2010 it collected about 3×10^{10} such muons with a median energy of $\simeq 20$ TeV which provides sufficient statistics to be sensitive to CR anisotropies down to a level of $\sim 10^{-4}$ at degree scales and above [41]. This revealed anisotropies at a level of $\simeq 10^{-3}$ on scales between 10° and 30° on the Northern hemisphere. Anisotropies on a similar level and with a consistent structure were also observed by the Tibet AS γ array, the Super-Kamiokande Detector, the Milagro Gamma Ray Observatory, and the ARGO-YBJ and EAS-TOP experiments (see Ref. [41] for references). Anisotropies at a similar level, but with a different structure on the sky was also observed up to energies of $\simeq 400$ TeV [42, 43]. This can be explained by diffusion in the turbulent Galactic magnetic field.

No significant anisotropies have been observed between $\simeq 10^{15}$ eV and up to the onset of the GZK threshold energy around a few times 10^{19} eV (see section 4 below) above which UHECRs lose energy within about 20 Mpc and sources must be located roughly within this distance scale.

In the UHECR regime, the Pierre Auger Observatory which observes the Southern hemisphere from Argentina has accumulated enough statistics to detect first signs of anisotropy: A significant correlation with the 12th edition of the Véron-Cetty and Véron catalog of nearby AGNs was observed for events with energies above 56 EeV [44]. This is very suggestive because this is essentially the same threshold energy above which the GZK effect limits the range of primary cosmic rays to ~ 50 Mpc. This does not necessarily mean that the Véron-Cetty and Véron catalog AGNs are the long sought UHECR sources, but it suggests that the real UHECR sources follow an anisotropic distribution similar to the one of nearby AGNs. Perhaps not surprisingly the sources may be astrophysical accelerators which follow the local large scale structure. Unfortunately, with accumulation of more data, these correlations have weakened somewhat [45]. The fraction of events above 55 EeV correlating with the Veron Cetty Catalog has come down from $69^{+11}_{-13}\%$ to $38^{+7}_{-6}\%$ compared to 21% expected for isotropy, while at the same time the statistical significance has stayed roughly constant at $\simeq 99\%$ confidence level. If one divides the sky distribution into an isotropic component and a component correlating, for example, with the 2MASS redshift survey, this corresponds to a relatively large isotropic fraction of 60–90% [45]. There is also a significant excess correlations seen with the 2MASS redshift survey. On the other hand, observations by the HiRes and Telescope Array experiments in the Northern hemisphere [46, 47] are so far consistent both with isotropy and with the fraction of events observed by the Pierre Auger Observatory that correlate with the Veron Cetty Catalog.

An interesting argument linking UHECR sources to their luminosity at radio frequencies has been put forward in this context by Hardcastle [48]. He concludes that if UHECRs are predominantly protons, then very few sources should contribute to the observed flux. These sources should be easy to identify in the radio and their UHECR spectrum should cut off steeply at the observed highest energies. In contrast, if the composition is heavy at the highest energies then many radio galaxies could contribute to the UHECR flux but due to the much stronger deflection only the nearby radio galaxy Centaurus A (“Cen A”) may be identifiable.

The Pierre Auger data does indeed show a clustering of super-GZK events towards the direction of Centaurus A (NGC 5128) [45]. This is somewhat surprising since, although Cen A is the closest radio galaxy at a distance of just $\simeq 3.6$ Mpc and the third-strongest radio source in the sky, it is an elliptical radio galaxy with a relatively small power output [50] which makes it difficult to reach the required UHECR energies. On the other hand, UHECR events observed towards Cen A could originate mainly from sources within the Centaurus galaxy cluster which is itself part of the Hydra-Centaurus supercluster and located just behind Cen A. In any case, Cen A has been observed in many channels and its small distance allows detailed astronomical and astrophysical studies. For example, its lobes have been detected in 200 MeV gamma-rays by Fermi Large Area Telescope

(Fermi LAT) [51], and its core was observed by Fermi LAT [52]. Such observations and its potential role as a major local UHECR accelerator has triggered many multi-messenger model building efforts for Cen A [50, 53]. For example, it has been pointed out in Ref. [53] that proton acceleration in the jet of Cen A is hard to reconcile with observations of Cen A in TeV gamma-rays by the H.E.S.S. telescopes [54] if gamma-rays are produced by proton-proton interactions. Instead, $p-\gamma$ interactions in the core are more consistent with these observations. We note that no significant excesses have been observed toward other directions on the sky where one could expect an overdensity of potential UHECR accelerators. For example, the Virgo cluster at a distance of $\simeq 20$ Mpc, thus within the GZK horizon, contains the prominent radio galaxy M87 but shows no excess UHECR flux [49].

4. – Propagation and Deflection

4.1. Galactic Cosmic Rays. – Galactic cosmic rays at least up to energies around the knee are deep in the diffusive regime in which their propagation can be described by solving a diffusion-convection-energy loss equation for the location- and energy dependent CR density per energy interval $n_i = n_i(\mathbf{r}, p)$ of a nuclear species i which depends on location and energy. It has the following general form,

$$(37) \quad \partial_t n_i = \partial_a (D_{ab} \partial_b - \mathbf{v}_{ca}) n_i + \partial_p \left(p^2 D_{pp} \partial_p \frac{n_i}{p^2} \right) - \partial_p \left[\dot{p} n_i - \frac{p}{3} (\nabla \cdot \mathbf{v}_c n_i) \right] + \sum_{j>i} \beta n_{\text{gas}} \int dp' \sigma_{j \rightarrow i}(p, p') n_j(p') - \beta \sigma_i(p) n_{\text{gas}} + \Phi_i,$$

where β is the CR velocity, D_{ab} is the diffusion tensor, $\mathbf{v}_c(\mathbf{r})$ is the convection velocity of the galactic plasma, $D_{pp}(\mathbf{r}, p)$ describes diffusion in momentum space and can give rise to re-acceleration, $\dot{p}(p)$ describes energy loss processes, $\sigma_{j \rightarrow i}(p, p')$ is the cross section for producing species i by spallation of species j upon interaction with the gas of density $n_{\text{gas}}(\mathbf{r})$, $\sigma_i(p)$ is the total inelastic cross section for interactions with the gas and $\Phi_i(\mathbf{r}, p)$ is the CR injection rate density per energy interval. To avoid clutter, in Eq. (37) we have only kept the dependencies on \mathbf{r} and p which are essential for an unambiguous definition of the various terms.

In general, Eq. (37) has to be solved numerically within a given geometry for the galactic disc which often is approximated as a slab with cylindrical symmetry such that all quantities only depend on r and z . In addition, assuming isotropic spatial diffusion with $D_{ab}(\mathbf{r}, p) = \delta_{ab} D(\mathbf{r}, p)$ in a turbulent magnetic field the scalar diffusion coefficient can be parametrized as

$$(38) \quad D(\mathbf{r}, p) = D_0 \beta \left(\frac{p/Z}{\text{GV}} \right)^\delta f(r, z),$$

with the rigidity p/Z in units of GigaVolts and where $f(r, z)$ is often taken as $f(r, z) \propto \exp(|z|/z_0)$, with z_0 the disc scale height. Under these assumptions and within quasilinear

theory the momentum diffusion coefficient is related to D by [55]

$$(39) \quad D_{pp}(p) = \frac{4v_A^2 p^2}{3\delta(4 - \delta^2)(4 - \delta)D(p)}.$$

There are several public program packages available such as GalProp [56] and DRAGON [57] for solving Eq. (37) in this scenario. The parameters δ and D_0/z_0 can be fixed by measuring secondary to primary CR ratios such as the boron to carbon or the nitrogen to oxygen ratio [58]. Typical values are $\delta \simeq 0.4\text{--}0.5$ and $D_0/z_0 \simeq (0.6\text{--}1) \times 10^{28} \text{ cm}^2 \text{ s}^{-1} \text{ kpc}^{-1}$.

With this we can now make a very simple argument linking the Galactic CR spectrum injected at the sources and the one observed at Earth: The supernova remnants that are thought to accelerate Galactic cosmic rays are now routinely observed in γ -rays and typically have a spectrum $\propto E^{-\alpha}$ with $\alpha \simeq 2.2$. It is also thought that at least for some of these supernova remnants there is a significant, if not dominant hadronic contribution to the γ -ray emission in which primary protons and nuclei interact with the ambient gas [59, 60]. Since the cross section for this interaction depends on energy only logarithmically, the slopes of the observed γ -ray spectrum and of the primary cosmic ray spectrum emitted by the sources should be essentially equal. An acceleration spectrum $\propto E^{-\alpha}$ with $\alpha \simeq 2.2$ is also consistent with non-relativistic shock acceleration theory, as we have seen in chapter 2. Assuming simple diffusion within a “leaky box” of height $\simeq 2z_0$ with a diffusion coefficient $D(p) \propto p^\delta$ that is spatially constant within the box, the *confinement time* in the Galactic disk can be estimated as $T_{\text{conf}}(p) \propto z_0^2/D(p) \propto p^{-\delta}$. Therefore, the charged cosmic ray spectrum observed at Earth $n(p)$ and the injected spectrum per volume $\Phi(p) \propto p^{-\alpha}$ are related by

$$(40) \quad n(p) \sim \Phi(p) T_{\text{conf}}(p) \propto \frac{\Phi(p)}{D(p)} \propto p^{-\alpha-\delta}.$$

For $\alpha \simeq 2.2$, as observed through the γ -rays, and $\delta \simeq 0.5$ for the power law index of the energy dependence of the diffusion coefficient, as inferred from Galactic CR nuclei abundances, this gives $n(p) \propto p^{-2.7}$ which is roughly consistent with observations, see Fig. 1.

4.2. Extra-Galactic Cosmic Rays. – We first discuss the main interaction processes of extragalactic hadronic UHECR here; the interactions of secondary γ -rays and neutrinos are the subject of section 7. Besides redshift which leads to a continuous decrease of the absolute momentum, $dp/dt = H(z)p$, with $H(z)$ the Hubble constant at a given redshift z , hadronic UHECR can interact with non-relativistic baryons in the form of gas or with low energy target photons. UHECR interactions with Galactic and extragalactic gas correspond to a cross section of order 0.1 barn, leading to an interaction time scale of order $\sim 10^{14} (n_g/10^{-6} \text{ cm}^{-3}) \text{ yr}$, with n_g the gas density. In general this has a negligible influence on UHECR propagation, except possibly in the centers of galaxy clusters or when secondary γ -rays and neutrinos from hadronic interactions are considered. Interactions with low energy photons includes Compton scattering, which is also negligible,

pair production, also known as Bethe-Heitler process, pion production and, for nuclei, photo-disintegration. In the following we consider the latter three processes.

The interaction length $l(E)$ of a CR of energy E and mass m propagating through a background of target photons is given by

$$(41) \quad l(E)^{-1} = \int d\varepsilon n_b(\varepsilon) \int_{-1}^{+1} d\mu \frac{1 - \mu\beta}{2} \sigma(s) = \frac{1}{2\gamma^2} \int d\varepsilon \frac{n_b(\varepsilon)}{\varepsilon^2} \int_0^{2\gamma\varepsilon} d\varepsilon' \varepsilon' \sigma(\varepsilon'),$$

where $n_b(\varepsilon)$ is the number density of the target photons per unit energy at energy ε , $\beta = (1 - m^2/E^2)^{1/2}$ is the CR velocity, μ is the cosine of the angle between the incoming momenta, $\gamma = E/m$ is the CR Lorentz factors and $\sigma(s)$ is the total cross section of the relevant process for the squared center of mass (CM) energy

$$(42) \quad s = m_b^2 + m^2 + 2\varepsilon E(1 - \mu\beta) = 2m\varepsilon'.$$

The last expressions in Eqs. (41) and (42) result from a Lorentz transformation to the CR rest frame in which the photon has energy ε' . This form is particularly useful when using data from laboratory measurements which are usually performed in the rest frame of the nucleus, such that the cross sections $\sigma(s)$ are usually known as functions of ε' . The most relevant target photon backgrounds turn out to be the infrared, the CMB, and the radio background. A review of the universal photon background has been given in Ref. [61].

The effective energy loss rate dE/dt is given by multiplying the integrand in Eq. (41) by $E\eta(s)$ where the inelasticity $\eta(s)$, i.e. the fraction of the energy transferred from the incoming CR to the recoiling final state particle of interest, is given by

$$(43) \quad \eta(s) \equiv 1 - \frac{1}{\sigma(s)} \int dE' E' \frac{d\sigma}{dE'}(E', s),$$

where E' is the energy of the recoiling particle considered in units of the incoming CR energy E . Here by recoiling particle we usually mean the “leading” particle, i.e. the one which carries most of the energy.

Pair production by a nucleus ${}_Z^A$ with mass number A and charge Z on a photon γ , ${}_Z^A\gamma \rightarrow {}_Z^A e^+e^-$, has a threshold energy of

$$(44) \quad E_{\text{npp}} = \frac{m_e(m + m_e)}{\varepsilon} \simeq 4.8 \times 10^{17} A \left(\frac{\varepsilon}{10^{-3} \text{ eV}} \right)^{-1} \text{ eV},$$

where $\varepsilon \sim 10^{-3} \text{ eV}$ represents the energy of a typical target photon such as a CMB photon. The inelasticity is very small, $\eta \sim 10^{-3}$, such that pair production can be treated as a continuous energy loss process with energy loss rate [62]

$$(45) \quad \left. \frac{dE_{A,Z}}{dt} \right|_{\text{NPP}} = - \frac{3\alpha Z^2 \sigma_T (m_e T_b)^2}{(2\pi)^3} f\left(\frac{m_e}{2\gamma T_b}\right).$$

Here, we have assumed a thermal background of temperature T_b because the CMB is by far the dominating background, $\alpha \simeq 1/137$ is the fine structure constant, $\sigma_T \equiv e^4/(6\pi m_e^2)$ is the Thomson cross section, and $f(x)$ is a function that was parametrized in Refs. [63, 64].

Let us next discuss pion production by UHE nucleons. The threshold for the reaction $N\gamma \rightarrow N\pi$, for a head-on collision of a nucleon N of energy E and mass m_N with a photon of energy ε is given by

$$(46) \quad E_{N\pi} = \frac{m_\pi(m_N + m_\pi/2)}{2\varepsilon} \simeq 3.4 \times 10^{19} \left(\frac{\varepsilon}{10^{-3} \text{ eV}} \right)^{-1} \text{ eV},$$

The pion production cross section that enters Eq. (41) and (43) has a threshold $\varepsilon' \simeq 150 \text{ MeV}$ in the nucleon rest frame, has a resonance at $\varepsilon' \simeq 350 \text{ MeV}$ with a peak value of $\sigma_{N\pi}(350 \text{ MeV}) \simeq 600 \mu\text{b}$ and an asymptotically almost constant cross section $\sigma_{N\pi}(\varepsilon' \gtrsim \text{GeV}) \simeq 150 \mu\text{b}$ in the multi-pion production regime. The inelasticity is $\simeq 20\%$ close to the threshold and $\simeq 50\%$ far above the threshold. Also, there is a channel which conserves the charge of the original nucleon, and one in which a proton turns into a neutron and a neutron turns into a proton. The charge conserving channel produces mostly neutral pions which decay into secondary γ -rays, whereas charge exchange reactions produce mostly charged pions which eventually decay into secondary electrons or positrons and neutrinos. These are the main production channels of secondary photons and neutrinos by hadronic cosmic rays, either within the sources, or during propagation to the observer, as we will see in more detail in section 7. Pion production is often modelled with the help of the numerical package SOPHIA [65].

To good approximation pion production by nuclei can be described in the *superposition model* in which nuclei are treated as a superposition of Z free protons and $A - Z$ free neutrons and their binding energy is neglected. Then the cross section for the reaction ${}_Z^A\gamma \rightarrow {}_Z^A\pi$ is given by

$$(47) \quad \sigma_{{}_Z^A\pi}(E) = Z\sigma_{p\pi}(E/A) + (A - Z)\sigma_{n\pi}(E/A).$$

Note that the energy carried away by a pion in such an interaction is $\sim 20\%$ of the interaction nucleon energy, hence only $\sim 20\%/A$ of the primary nucleus. The threshold for photo-pion production is also increased to $\simeq 4 \cdot 10^{19} \times \text{AeV}$.

The range of energies for the photodisintegration process, in terms of the photon energy ε' in the rest frame of the nucleus, splits into two parts. The first contribution comes from the low energy range up to 30 MeV , in the Giant Dipole Resonance region, where emission of one or two nucleons dominates; the second contribution comes from energies between 30 MeV and 150 MeV , where multi-nucleon energy losses are involved. These processes have first been discussed in some detail in Ref. [62]. More recent descriptions can be found in Refs. [66]. In a photodisintegration event the changes in energy, ΔE , and atomic number, ΔA , are related by $\Delta E/E = \Delta A/A$. Thus, the effective energy loss

rate due to photodisintegration $\left. \frac{dE}{dt} \right|_{\text{eff,photo}}$ is given by

$$(48) \quad \frac{1}{E} \left. \frac{dE}{dt} \right|_{\text{eff,photo}} = \frac{1}{A} \frac{dA}{dt} = \sum_i \frac{i}{A} l_{A,i}(E),$$

where $l_{A,i}(E)$ is the mean free path Eq. (41) for emission of i nucleons.

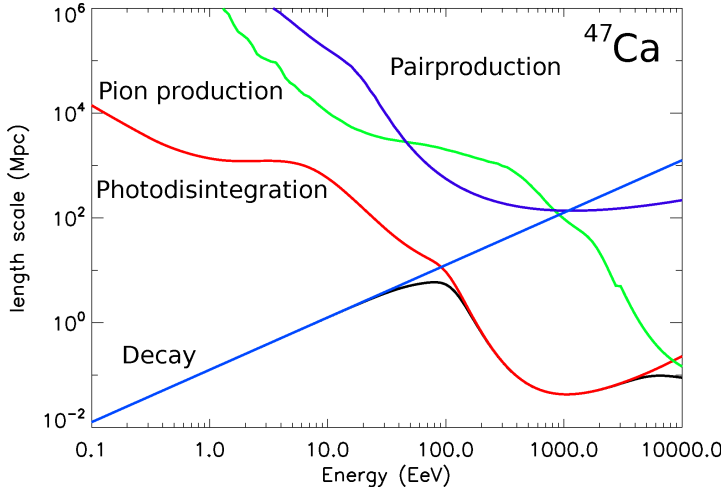


Fig. 5. – The length scales for all relevant processes of the example nucleus ^{47}Ca as a function of energy: Energy loss length for pair production, decay length, and mean free path for pion production and photodisintegration.

Fig. 5 shows the lengths scales for all relevant interactions for the example nucleus ^{47}Ca .

The amount of deflection of extragalactic cosmic rays in cosmic magnetic fields is still hard to quantify. In a field with rms strength B and coherence length l_c the rms deflection angle of a cosmic ray of energy E and charge Ze traveling a distance d is given by [67]

$$(49) \quad \theta(E, d) \simeq \frac{(2dl_c/9)^{1/2}}{r_g} \simeq 0.8^\circ Z \left(\frac{E}{10^{20} \text{ eV}} \right)^{-1} \left(\frac{d}{10 \text{ Mpc}} \right)^{1/2} \left(\frac{l_c}{1 \text{ Mpc}} \right)^{1/2} \left(\frac{B}{10^{-9} \text{ G}} \right),$$

in the small deflection angle limit $\theta(E, d) \ll 1$, where r_g is again the gyro radius of Eq. (6). The dependence on the dimension-full quantities can be easily understood from the fact that the deflection angles $\theta_1 \simeq l_c/r_g$ accumulated in individual domains of size l_c in which the magnetic field can be approximated as being constant, are uncorrelated between different domains and thus have to be added in quadrature.

For an order of magnitude estimate for the deflection angles in the Galactic magnetic field we use $l_c \sim 100$ pc, $d \sim 10$ kpc, $B \sim 3 \mu\text{G}$ gives $\theta(E) \sim 1^\circ Z(10^{20} \text{ eV}/E)$. Thus, protons around the GZK cut-off, $E \sim 60$ EeV, will be deflected by a few degrees or less, whereas iron nuclei can be deflected by several tens of degrees. This implies that Galactic magnetic fields are likely to destroy any possible correlation with the local large scale structure in case of a heavy composition. Numerical simulations using detailed models of the Galactic magnetic field, including a turbulent component, demonstrate that the relatively large deflections of UHECR nuclei in the Galactic magnetic field can considerably distort the images of individual sources. If UHECR source follow the local large scale structure its image can also be distorted and shifted considerably [68].

Deflection of UHECRs in cosmic magnetic fields goes along with a time delay compared to the light travel time, which can be quantified by [67]

$$\tau(E, d) \simeq d\theta(E, d)^2/4 \simeq 1.5 \times 10^3 Z^2 \left(\frac{E}{10^{20} \text{ eV}} \right)^{-2} \left(\frac{d}{10 \text{ Mpc}} \right)^2 \left(\frac{l_c}{1 \text{ Mpc}} \right) \left(\frac{B}{10^{-9} \text{ G}} \right)^2 \text{ yr}, \quad (50)$$

which, up to numerical factors, follows from elementary geometry of an arc of length d curving with an angle $\theta(E, d)$. This has interesting consequences for UHECR sources that are variable or bursting on time scales comparable or smaller than $\tau(E, d)$: Provided that the time scale over which the UHECR sky is observed (typically over a few years) is smaller than $\tau(E, d)$, the observable spectrum from such an intermittent source will be peaked around a specific energy, independent of the actual source spectrum: Higher-energy particles would have passed the observer already, whereas lower-energy particles would not have arrived yet. This could happen in particular for GRB sources.

Large scale extra-galactic magnetic fields (EGMF) are much less well known than Galactic magnetic fields [69]. One of the major detection methods for the EGMF is to measure the Faraday rotation of the polarization of radio emission from a distant source which is proportional to the line of sight integral of the product of the plasma density and the parallel magnetic field component. These so called Faraday rotation measures are only sensitive to magnetic fields stronger than $\sim 0.1 \mu\text{G}$, whereas fields down to \sim nano Gauss still have significant effects on UHECR deflection, according to Eq. (49). To measure Faraday rotations in such weaker fields requires much higher statistics than is currently available. The statistical average over the sky of an all pervading EGMF is currently constrained to be $\lesssim 3 \times 10^{-7} (l_c/\text{Mpc})^{1/2} \text{ G}$ [70]. Assuming an EGMF whose flux is frozen into the highly conducting plasma of the intergalactic medium and thus follows the large scale structure gives the more stringent limit $B \lesssim 10^{-9} - 10^{-8} \text{ G}$ for an all pervading field. At the same time, the fields in the sheets and filaments of the galaxy distribution can in this case be as strong as a micro Gauss. Fields of that strength are also routinely observed in galaxy clusters which are the largest virialized structures in the Universe. Outside of galaxy clusters there are currently at most hints of an EGMF, for example in the Hercules and Perseus-Pisces superclusters [71]. Within the next 10-15 years, large scale radio telescopes such as Lofar and SKA are, however, expected to dramatically improve observational information on the EGMF in the large scale structure.

From the theoretical point of view, the EGMF in the voids are expected to be very weak and uncontaminated by astrophysical processes. This makes voids excellent probes of relic magnetic seed fields that may have been created in the early Universe [72]. It is very interesting in this context that the non-observation at GeV energies by the Fermi LAT satellite experiment of certain distant blazars that have been detected at TeV energies by the ground based H.E.S.S. experiment suggest a *lower limit* $B \gtrsim 3 \times 10^{-16}$ G on the EGMF in the voids [73]. This is because the TeV gamma-rays observed by H.E.S.S. would initiate electromagnetic cascades that should be detectable by Fermi unless an EGMF of strength $B \gtrsim 3 \times 10^{-16}$ G deflects the electrons and positrons in these cascades into a diffuse halo around the source whose flux is then below the Fermi LAT sensitivity. We note in this context, however, that magnetic fields $\lesssim 10^{-12}$ G are not relevant for UHECR propagation.

While waiting for more observational information on the EGMF, another approach for quantifying the effects of large scale cosmic magnetic fields on UHECR propagation is to build models of the EGMF using large scale structure simulations. Two major techniques used in this context are a magnetohydrodynamic (MHD) version of a constrained smooth particle hydrodynamics code [74] and Eulerian grid-based hydro+n-body codes [75]. The magnetic fields are followed by solving the MHD equations in the ambient plasma while neglecting back-reaction onto the plasma. Since the MHD equations are linear in the magnetic field, a seed field is required which is assumed to be either uniform or concentrated around cosmic shocks, for example at accretion shocks around galaxy clusters, where they could arise astrophysically, for example, through the Biermann battery mechanism. The magnetic field is then normalized such that it approximately reproduces the largest fields observed in galaxy clusters. Alternatively, it has been assumed that the EGMF follows the local vorticity and turbulent energy density of the intergalactic plasma [76]. All these numerical approaches agree on the fact that these fields tend to follow the large scale galaxy distribution such that they tend to be strongest around the largest matter concentrations. A cross section through one of these simulations [77, 78] is shown in Fig. 6 (upper panel). On the other hand, numerical models disagree on certain aspects that are relevant for UHECR deflection, most notably the distribution of filling factors, i.e. the fraction of space filled with EGMF above a certain strength, as a function of that strength [79]. While this can cause considerable differences in the size of the deflection angles predicted between the source and the observed events, before impinging on the Galactic magnetic field, the UHECR arrival directions should still follow the large scale galaxy distribution because the deflections tend to be *along and within* the cosmic large scale structure. This is demonstrated in Fig. 7 where the deflected UHECR arrival directions tend to follow arc-like structures that result from deflections within the large scale cosmic filaments. In other words, the EGMF is unlikely to deflect UHECRs out of the large scale structure since the fields in the voids are very small. Furthermore, the local group of galaxies is a relatively inactive region and not strongly magnetized such that extragalactic deflection within $\simeq 1\text{--}2$ Mpc is likely to be small. This means that while the events will in general not point back to their sources, the arrival direction distribution of UHECRs coming from outside the Galaxy is likely to still correlate with the local large

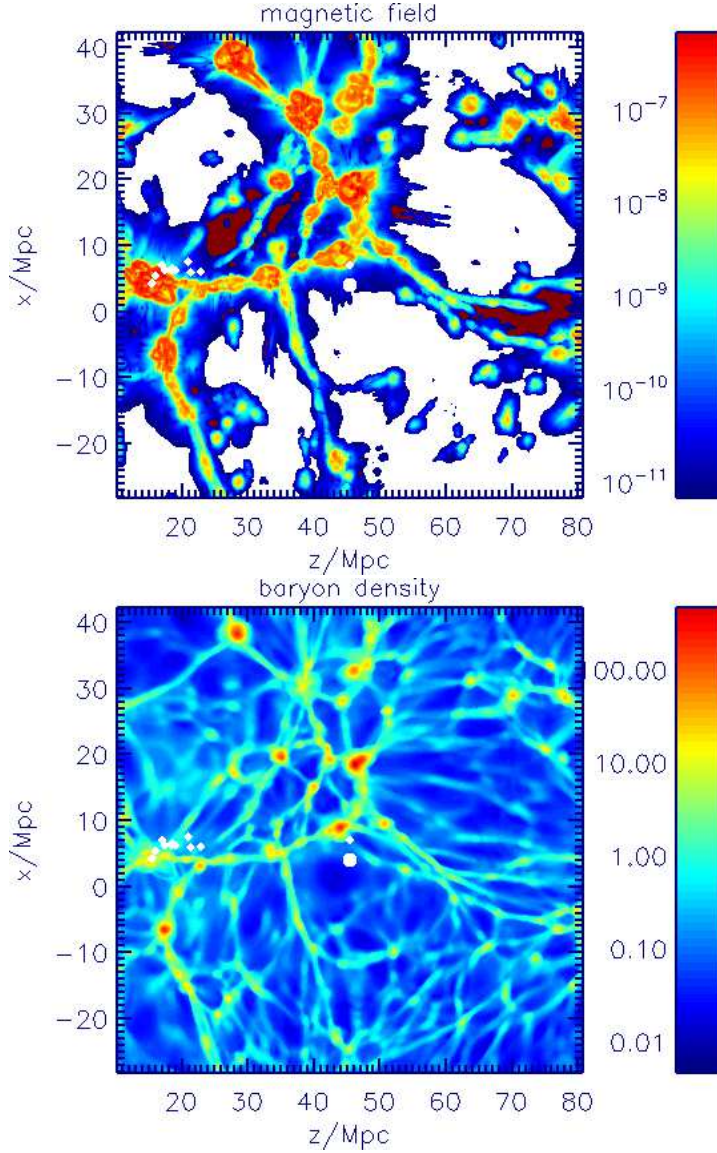


Fig. 6. – A cross section through the large scale structure simulation from Ref. [77, 78] on a scale of 70 Mpc in both directions. Ten sources are marked with white diamonds in the environment of a massive galaxy cluster. The white sphere of radius 1 Mpc indicates the observer and right above marked as a further white diamond is a nearby source. Upper panel: Magnetic field strength as color contours in units of Gauss, as indicated. Lower panel: Baryon density is color contours in units of average density.

scale structure even in scenarios with strong EGMF, heavy nuclei and large deflection

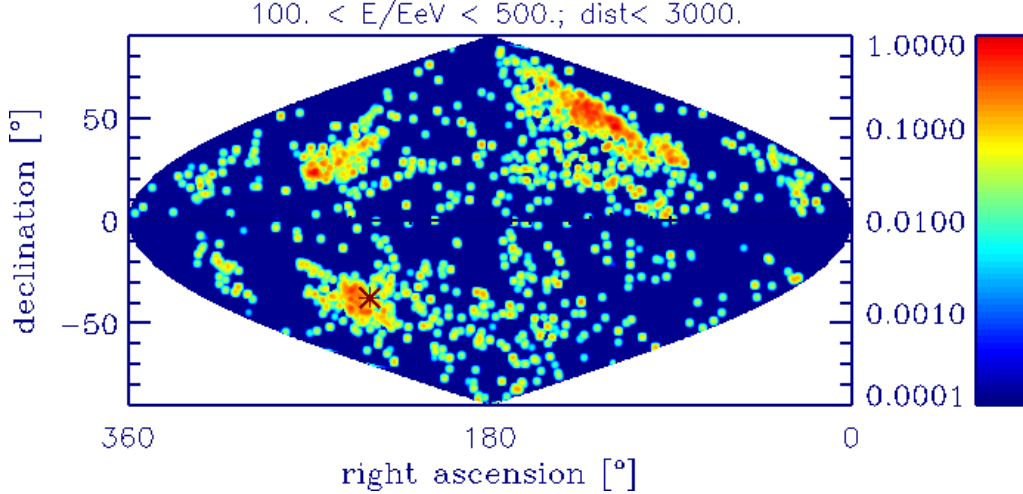


Fig. 7. – Simulated arrival directions of UHECR above 10^{20} eV in a scenario where the sources shown in Fig. 6 inject mostly protons with a small admixture of a fraction of $x_{26,56} = 6.83 \times 10^{-4}$ iron nuclei at given energy per nucleon, E/A , roughly corresponding to the galactic abundance of iron. Acceleration is taken to be rigidity limited power law $\Phi_{Z,A}(E) = dN_{Z,A}/dE \propto q_{Z,A} E^{-2.7} \Theta(Z E_{\max,p} - E)$ with $E_{\max,p} = 3.85 \times 10^{20}$ eV, where according to Eq. (25) the iron abundance at given energy E is $q_{26,56} = 0.64$. All sources are assumed to have equal luminosity. The star marks the location of the prominent galaxy cluster in the middle left part of the cross sections in Fig. 6

angles. Therefore, for a heavy composition the main effect on correlations with the local large scale structure will come from the in this case substantial deflections in the Galactic magnetic fields which should not correlate with extragalactic deflections.

Structured EGMF can also have considerable effects on spectrum and composition of the cosmic ray spectrum at energies $\sim 10^{18}$ eV and below, in particular for sources within strongly magnetized structures: The magnetic fields in galaxy clusters reach micro-Gauss strength over the core regions which can stretch over several 100 kpc, with coherence lengths of 10–100 kpc. Eq. (50) then implies that UHECR of energy $E \lesssim \text{few} \times Z \times 10^{17}$ eV will remain confined during the lifetime $\lesssim 10^{10}$ yr of the galaxy cluster. This can have two effects: First, below these energies the spectrum from such sources will be strongly suppressed, which amounts to a “magnetic horizon effect” [80, 81]. Second, the mass composition at a given energy in this range can be strongly shifted to a light composition compared to the injected composition because heavier ions are confined longer and thus more heavily suppressed.

The simulations for Fig. 7 have been performed with the public software package CR-Propa [82, 83] which can propagate of UHE nuclei with and without deflection, including secondary electromagnetic cascades and neutrinos.

5. – Mass Composition

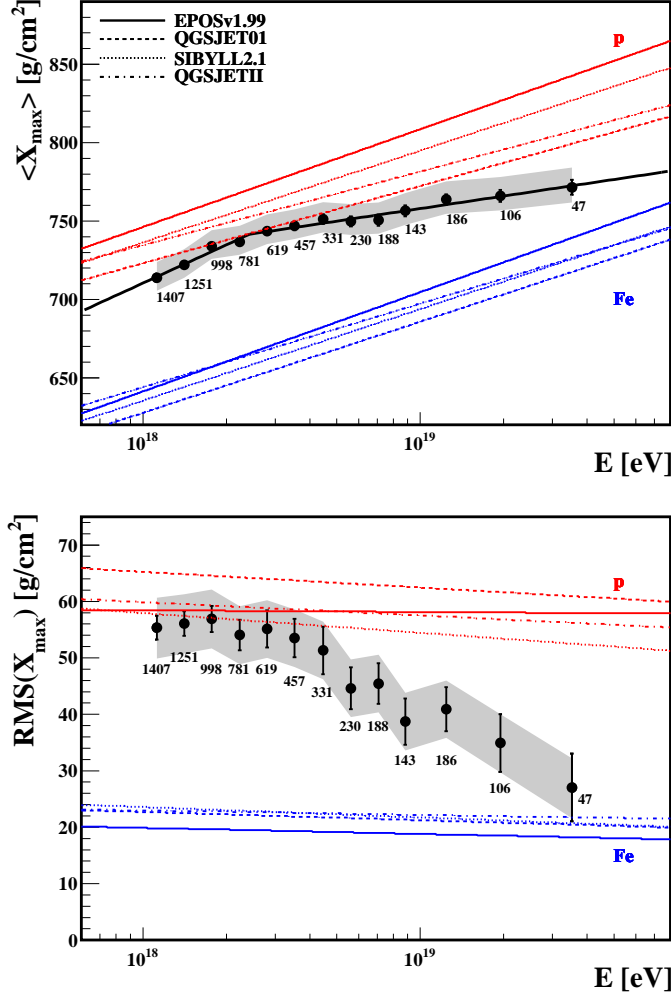


Fig. 8. – Air shower data from the Pierre Auger Observatory: The average atmospheric depth at which the showers in a given energy bin peak (upper panel) and its root mean square (lower panel), as a function of energy, compared to the predictions of different air shower simulations for proton (red, upper curves) and iron primaries (blue, lower curves). Plots are taken from Ref. [85].

Another interesting new question concerns the mass composition of highest energy cosmic rays: The depth in the atmosphere where particle density in the giant air showers observed by the Pierre Auger Observatory is maximal, and in particular the fluctuations of the depth of shower maximum from event to event, when compared with air shower

simulations, point towards a composition that gradually becomes heavier with increasing energies [84, 85], as is evident in Fig. 8. It is also interesting to note in this respect that there is a tension between the average atmospheric depth and its fluctuation at the highest energies, when interpreted within the hadronic interaction models shown in Fig. 8: Whereas the average depth hints at a mixed composition with a significant light component, the observed fluctuations become so small that they would be more consistent with an almost pure iron composition.

On the other hand, HiRes observations are consistent with a light composition above $\simeq 1.6 \times 10^{18}$ eV and up to $\simeq 5 \times 10^{19}$ eV above which statistics is insufficient to determine composition [86]. This could indicate that statistics is still too limited to draw firm conclusions or that the Northern and Southern hemispheres are significantly different in terms of UHECR composition. In addition, there are significant uncertainties in hadronic cross sections, multiplicities and inelasticities and none of the existing hadronic interaction models consistently describes the shower depth and muon data of the Pierre Auger experiment [87, 88]. Note that the center of mass energy for a UHECR interacting in the atmosphere reaches a PeV = 10^{15} eV, which is still a factor of a few hundred higher than the highest energies reached in the laboratory, at the Large Hadron Collider (LHC) at CERN. It is, therefore, not excluded that the true mass composition is light on both hemispheres and the UHECR data teaches us something about hadronic interactions at energies unattainable in the laboratory.

The question of mass composition is linked to other observables such as the UHECR spectrum. Unfortunately, the current statistics is still insufficient to gain significant information on the mass composition from the observed spectrum. The flux suppression observed above $\simeq 4 \times 10^{19}$ eV is qualitatively consistent with either proton or nuclei heavier than carbon up to iron nuclei [20, 89, 38]. In the latter case, the main energy loss process responsible for the “cut-off” is photo-disintegration on the CMB and infrared backgrounds. It should be noted, however, that the observed flux suppression could also be due to the intrinsic maximal acceleration energies attained in the sources, although it would possibly be somewhat of a coincidence that this energy should be close to the GZK energy.

6. – High Energy Neutrino Detection

Detection rates of high energy neutrinos will not only depend on their fluxes for which we have discussed various scenarios in the two previous two chapters, but also on their interaction cross section with the detector medium. We, therefore, will now discuss the scattering cross sections of neutrinos with ordinary matter.

Imagine a neutrino of energy E_ν scattering on a parton i carrying a fraction x of the 4-momentum P of a state X of mass M . Denoting the fractional recoil energy of X by $y \equiv E'_X/E_\nu$ and the distribution of parton type i by $f_i(x, Q)$, in the relativistic limit

$E_\nu \gg m_X$ the contribution to the νX cross section turns out to be

$$(51) \quad \frac{d\sigma_{\nu X}}{dx dy} = \frac{2G_F^2 M E_\nu x}{\pi} \left(\frac{M_{W,Z}^2}{2M E_\nu x y + M_{W,Z}^2} \right)^2 \sum_i f_i(x, Q) [g_{i,L}^2 + g_{i,R}^2 (1-y)^2] .$$

Here, $g_{i,L}$ and $g_{i,R}$ are the left- and right-chiral couplings of parton i , respectively. Eq. (51) applies to both charged and neutral currents, as well as to the case where X represents an elementary particle such as the electron, in which case $f_i(x, Q) = \delta(x-1)$.

As usual, if the four-momentum transfer Q becomes comparable to the electroweak scale, $Q^2 \gg M_{W,Z}^2$, the weak gauge boson propagator effects, represented by the factor $M_{W,Z}^2/(Q^2 + M_{W,Z}^2)$ in Eq. (51), become important. We have used that in the limit $|Q^2| \gg M^2$ one has $0 \simeq -M^2 = (xP+Q)^2 \simeq Q^2 + 2P \cdot Q x$ with $P \cdot Q \simeq -ME'_X = -ME_\nu y$ evaluated in the laboratory frame, i.e. the rest frame of X before the interaction. $Q^2 \simeq 2ME_\nu xy$ is also called the *virtuality* because it is a measure for how far the exchanged gauge boson is from the mass shell $Q^2 = -M_{W,Z}^2$.

We will not derive Eq. (51) in detail, but it is easy to understand its structure: First, the overall normalization is analogous to the cross section in the four-fermion approximation,

$$(52) \quad \sigma(\bar{\nu}_e p \rightarrow n e^+) = \frac{G_F^2}{\pi} |M_{if}|^2 \frac{p_f^2}{v_i v_f} ,$$

using the fact that for $E_\nu \gg M$ the CM momentum $p_*^2 \simeq ME_\nu/2$. Second, if the helicities of the parton and the neutrino are equal, the total spin is zero and the scattering is spherically symmetric in the CM frame. In contrast, if the parton is right-handed, the total spin is 1 which introduces an angular dependence: After a rotation by the scattering angle θ_* in the CM frame the particle helicities are unchanged for the outgoing final state particle and one has to project back onto the original helicities in order to conserve spin. If a left-handed particle originally propagated along the positive z-axis, its left-handed component after scattering by θ_* in the $x-z$ plane is

$$(53) \quad \frac{1}{2} \left(1 - \frac{\boldsymbol{\sigma} \cdot \mathbf{p}}{p} \right) \begin{pmatrix} 0 \\ 1 \end{pmatrix} = \frac{1}{2} \begin{pmatrix} -\sin \theta_* \\ 1 + \cos \theta_* \end{pmatrix} ,$$

giving a projection $[(1 + \cos \theta_*)/2]^2$. Now, Lorentz transformation from the CM frame to the lab frame gives $E'_\nu/E_\nu = (1 + v_X \cos \theta_*)/2 \simeq (1 + \cos \theta_*)/2$ in the relativistic limit and thus the projection factor equals $(E'_\nu/E_\nu)^2 = (1 - E'_X/E_\nu)^2 = (1-y)^2$, as in Eq. (51) for the right-handed parton contribution. Integrated over $0 \leq y \leq 1$ this gives 1/3, corresponding to the fact that only one of the three projections of the $J=1$ state contributes.

We now briefly consider neutrino-nucleon interaction. From Eq. (51) it is obvious that for $2E_\nu m_N \ll M_{W,Z}^2$ the total neutrino-nucleon cross section is proportional to the neutrino energy E_ν . In the opposite, ultra-high energy limit $2E_\nu m_N \gg M_{W,Z}^2$, the

dominant contribution comes from partons with

$$(54) \quad x \sim \frac{M_{W,Z}^2}{2E_\nu m_N}.$$

Since, very roughly, $xf_i(x, Q) \propto x^{-0.3}$ for $x \ll 1$, it follows that the neutrino-nucleon cross section approximately grows $\propto E_\nu^{0.3}$. This is confirmed by a more detailed evaluation of Eq. (51) using the CTEQ4-DIS parton distributions [90]. A good power law fit is given by

$$(55) \quad \sigma_{\nu N}(E) \simeq 2.36 \times 10^{-32} (E/10^{19} \text{ eV})^{0.363} \text{ cm}^2 \quad (10^{16} \text{ eV} \lesssim E \lesssim 10^{21} \text{ eV}).$$

Let us use this to do a very rough estimate of event rates expected for extraterrestrial UHE neutrinos in neutrino telescopes. Such neutrinos are usually produced via pion production by accelerated UHE protons interacting within their source or with the cosmic microwave background (CMB) during propagation to Earth. At GZK energies the secondary neutrino flux should very roughly be comparable with the primary UHE cosmic ray flux, within large margins. This argument is actually known as “Waxman-Bahcall bound”, see Eq. (57) below. Using that the neutrino-nucleon cross section from Eq. (55) scales as $\sigma_{\nu N} \propto E_\nu^{0.363}$ for $10^{16} \text{ eV} \lesssim E_\nu \lesssim 10^{21} \text{ eV}$, and assuming water or ice as detector medium, we obtain the rate

$$(56) \quad \begin{aligned} \Gamma_\nu &\sim \sigma_{\nu N}(E_\nu) 2\pi E_\nu j(E_\nu) n_N V_{\text{eff}} \\ &\sim 0.03 \left(\frac{E_\nu}{10^{19} \text{ eV}} \right)^{-0.637} \left(\frac{E_\nu^2 j(E_\nu)}{10^2 \text{ eV cm}^{-2} \text{ sr}^{-1} \text{ s}^{-1}} \right) \left(\frac{V_{\text{eff}}}{\text{km}^3} \right) \text{ yr}^{-1}, \end{aligned}$$

where $n_N \simeq 6 \times 10^{23} \text{ cm}^{-3}$ is the nucleon density in water/ice, V_{eff} the effective detection volume, and $j(E_\nu)$ is the differential neutrino flux in units of $\text{cm}^{-2} \text{ eV}^{-1} \text{ sr}^{-1} \text{ s}^{-1}$.

Eq. (56) indicates that at $E_\nu \gtrsim 10^{18} \text{ eV}$, effective volumes $\gtrsim 100 \text{ km}^3$ are necessary. Although impractical for conventional neutrino telescopes, big air shower arrays such as the Pierre Auger experiment [91] can achieve this. In contrast, if there are sources such as active galactic nuclei emitting at $E_\nu \sim 10^{16} \text{ eV}$ at a level $E_\nu^2 j(E_\nu) \sim 10^2 \text{ eV cm}^{-2} \text{ sr}^{-1} \text{ s}^{-1}$, km-scale neutrino telescopes should detect something.

Nowadays there are several different techniques to detect high energy neutrinos [105]. The most conventional detects the Cherenkov emission of the high energy muons in water or ice that are produced by charged current interactions of muon neutrinos. Interactions which do not produce muons, namely neutral current interactions and charged current interactions of electron and tau-neutrinos, can also be detected via the electromagnetic and hadronic cascades initiated by the electrons and tau-leptons and by the energy-momentum transferred to the target nuclei. These two detection modes are sketched in Fig. 9. At the time of writing of this monograph, active experiments using this technique include the Lake Baikal neutrino telescope [92], the ANTARES neutrino telescope [93]

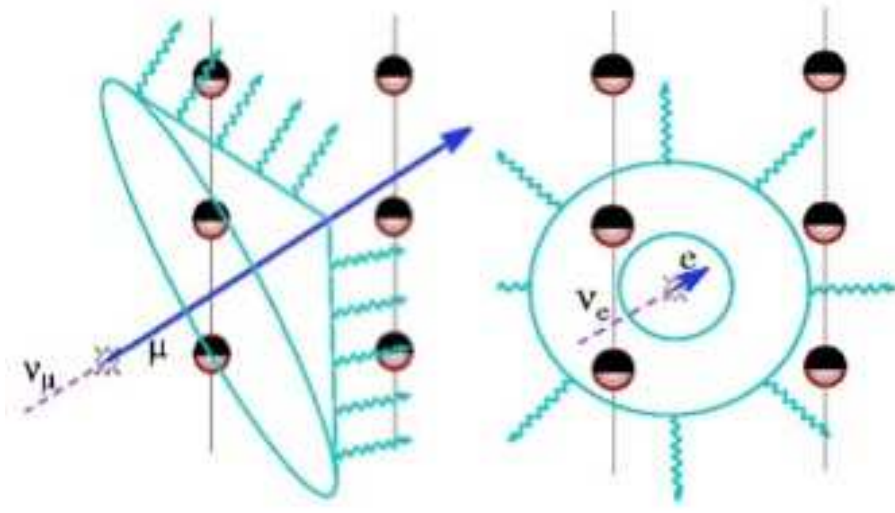


Fig. 9. – Left panel: Muon neutrino detection in water or ice by Cherenkov radiation of the muon produced by a charged current interactions. Right panel: Neutrino detection by electromagnetic and hadronic cascades.

which operates off the coast of Toulon in the Mediterranean sea and the IceCube telescope [40] in the ice beneath the South Pole, which is currently is the largest instrument and will reach a sensitivity of $E_\nu^2 j(E_\nu) \simeq 2 \text{ eV cm}^{-2} \text{ sr}^{-1} \text{ s}^{-1}$ to the diffuse neutrino flux between $\simeq 10^{14} \text{ eV}$ and $\simeq 2 \times 10^{16} \text{ eV}$ after 3 years of operation with 86 strings carrying a total of 5,160 optical modules. An infill is planned to lower the threshold down to about 10 GeV. Due to the large background of down-going atmospheric muons from cosmic ray interactions in the atmosphere above the detector, these instruments are usually optimized to detection of up-going neutrinos, which limits their energy range to $\lesssim 10^{16} \text{ eV}$ above which neutrinos get absorbed in the Earth. However, the atmospheric neutrino background becomes sufficiently small again above $\simeq 10^{17} \text{ eV}$ to detect down-going neutrinos. To complement IceCube which operates in the Southern hemisphere, there are plans to construct a km-scale neutrino telescope in the Northern hemisphere, based on the three smaller scale and water-based projects ANTARES, NEMO and NESTOR.

Neutrinos with energies above $\sim 10^{17} \text{ eV}$ can induce giant air showers in the atmosphere, just as charged cosmic rays and γ -rays do. However, due to their small cross section, the neutrino interaction probability in one vertical atmospheric depth is $\lesssim 10^{-4}$ even at the highest energies. Therefore, neutrino induced air showers are typically deeply penetrating (also called “horizontal”) or even Earth-skimming, which can be used to distinguish them from cosmic and γ -ray induced air showers. This is sketched in Fig. 10. The tau-neutrino is especially suitable for Earth-skimming showers because the tau-neutrino can produce a tau-lepton by a charged-current interactions which travels with little energy loss before decaying and inducing a giant air shower which can be de-

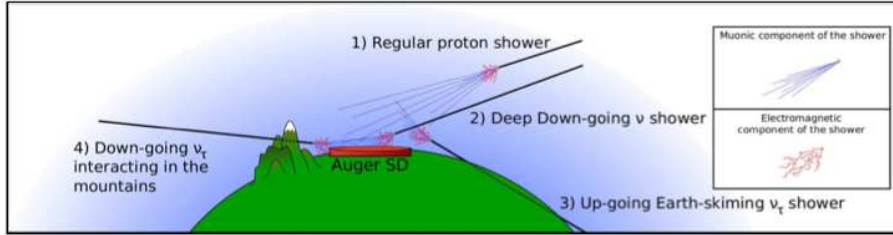


Fig. 10. – Sketch of the neutrino detection modes of the Pierre Auger Observatory (from Ref. [94]).

tected. In this detection mode, the decay length of the tau-lepton has to be comparable to the dimensions of the detector, which limits sensitivity to the energy interval between $\simeq 10^{17}$ eV and $\simeq 2 \times 10^{19}$ eV in case of the Pierre Auger Observatory [25]. In a water or ice based detector such as IceCube the neutrino charged current interaction can also be seen which gives rise to “double bang events” at energies around 10^{16} eV.

From the non-observation of Earth-skimming neutrinos the Pierre Auger experiment has put an upper limit of $E_\nu^2 j(E_\nu) \lesssim 30 \text{ eV cm}^{-2} \text{ sr}^{-1} \text{ s}^{-1}$ on the diffuse neutrino fluxes between $\simeq 10^{17}$ eV and $\simeq 2 \times 10^{19}$ eV [94, 91] that is comparable to the current IceCube limit [95] and also to the theoretical Waxman-Bahcall and cascade limits, see Eq. (57) and (58), respectively, below. In the future, neutrino induced air showers may also be observed from space which allows for a considerable increase of effective target mass. The JEM-EUSO experiment (“Extreme Universe Space Observatory onboard Japanese Experiment Module”) [96] is considered to be flown on the International Space Station (ISS). In the farther future one or several freely flying satellites could be used for UHE cosmic ray and neutrino detection.

We note in passing that the rate of horizontal neutrino induced air showers is proportional to the product of the flux and the neutrino-nucleon cross section because the atmosphere is transparent even to the highest energy neutrinos. In contrast, the rate of Earth skimming neutrinos tends to decrease with the neutrino-nucleon cross section due to shadowing in the Earth crust. This may allow to break the degeneracy of rates in fluxes and cross sections and thus would allow to measure the UHE neutrino-nucleon cross section once a sufficient number of both types of air showers are measured [97].

Finally, neutrinos can be detected from the radio emission of the charged particle showers they produce in the atmosphere or at surfaces of ice or rock: Since electrons created by ionization are more mobile than the positive charges of the nuclei, there will be an excess of electrons. In addition, the electrons interact differently than nuclei and positrons. The resulting moving charge cloud will emit coherent radio waves either by interactions with the Earth’s magnetic field, which is the main emission mechanism in the atmosphere, or via Cherenkov emission, known as the Askaryan effect, which dominates emission at ice and rock surfaces. The latter effect has been used to set upper limits on the UHE neutrino flux by several experiments such as ANITA [98] above $\simeq 10^{17}$ eV, a balloon

flying around the South Pole [99], and by observing the moon’s rim with radio telescopes such as the Westerbork Synthesis Radio Telescope (the NuMoon project) [100] above $\simeq 10^{22}$ eV. The use of radio telescopes for observing radio pulses induced by neutrinos on the moon’s surface will become in particular interesting with the arrival of Lofar [102] and SKA [103] and the latter would allow to lower the threshold to $\simeq 10^{20}$ eV. This technique can also be used for UHE cosmic rays [101]. There are further radio detection projects in Antarctica, such as ARIANNA, ARA and a ExaVolt Antenna (EVA) [104], a next-generation version of ANITA.

7. – High Energy Neutrino Fluxes

Fig. 11 shows the diffuse “grand unified” neutrino spectrum from the lowest energies corresponding to the cosmological relic blackbody spectrum of temperature $\simeq 1.9$ K to the highest energy neutrinos produced by interactions of UHECRs. In the following we will restrict ourselves to the high energy range at a TeV and above.

The interactions of UHECR in general also give rise to secondary neutrino and γ -ray fluxes. Therefore, the physics and astrophysics of UHECRs is also inextricably linked with the emerging field of neutrino astronomy [105] and with the already well established field of γ -ray astronomy [107]. In fact, neutrino and γ -ray observations and limits often already severely constrain scenarios of UHECR origin. In turn, this link plays an important role for theoretical predictions of fluxes of extragalactic neutrinos with energies above roughly a TeV whose detection is a major goal of several next-generation neutrino telescopes including IceCube at the South pole and the planned European KM3NeT. If such neutrinos are produced as secondaries of UHECRs accelerated in astrophysical sources and if these primary UHECRs are not absorbed within the sources, but rather directly contribute to the observed UHECR flux, then the energy fluence in the neutrino flux can not be higher than the one in UHECRs. This corresponds to the so called Waxman-Bahcall bound

$$(57) \quad E_\nu^2 \frac{dN_\nu}{dE_\nu} \lesssim (10 - 50) \text{ eV sr}^{-1} \text{ s}^{-1} \text{ cm}^{-2},$$

where the range of values is due to uncertainties in the cosmological evolution of the sources. The Waxman-Bahcall bound applies to sources which are transparent to the high energy cosmic rays they accelerate and which have acceleration spectra not much harder than E^{-2} [108, 109]. It does not hold if one of these assumptions does not apply. This includes cases such as acceleration sources with injection spectra considerably harder than E^{-2} , so called “hidden” sources which are opaque to the primary UHECRs that they accelerate, and top-down scenarios where UHECRs are produced by very heavy relic particles decaying mostly into γ -rays and neutrinos and only to $\sim 10\%$ into nucleons, rather than by acceleration. In such cases where the Waxman-Bahcall bound does not apply, the neutrino fluxes are still constrained by the observed diffuse γ -ray flux in the 100 GeV range. This is because neutrinos are predominantly produced through the decay of charged pions, due to approximate isospin symmetry of known pion production

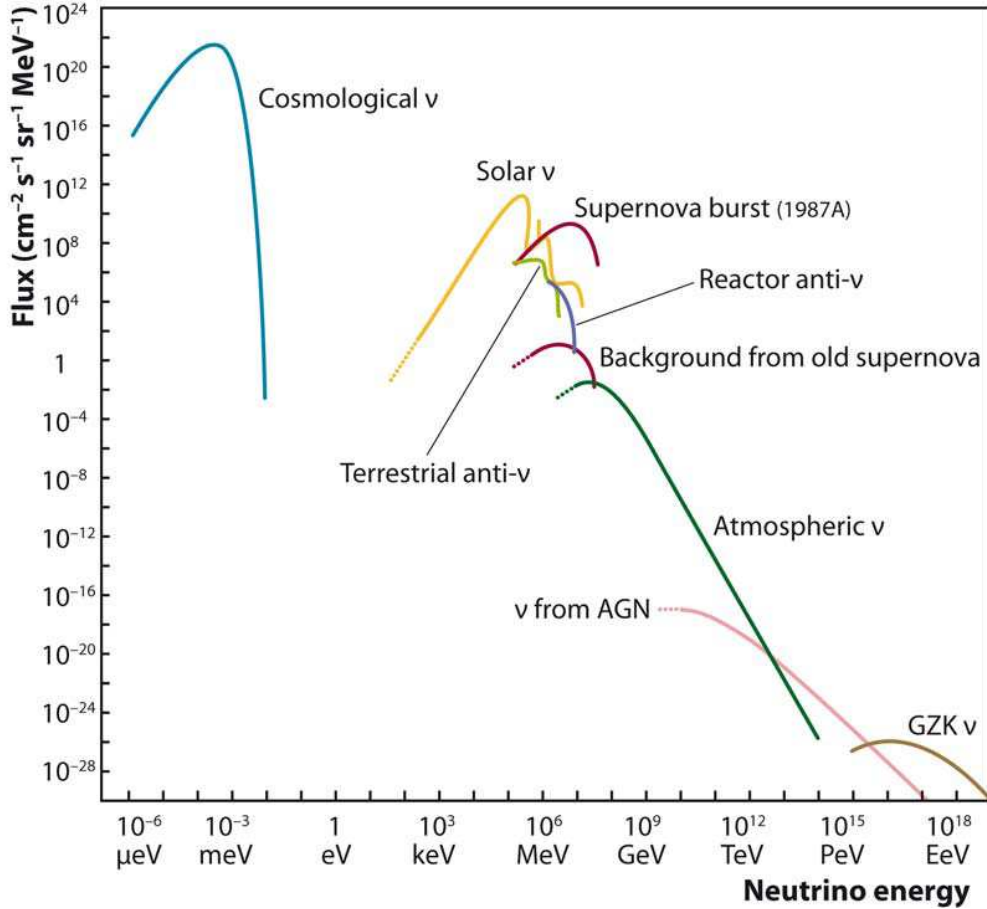


Fig. 11. – The diffuse “grand unified” neutrino spectrum. Solar neutrinos, a burst of neutrinos of a few seconds length from SN1987A, reactor neutrinos, terrestrial neutrinos and atmospheric neutrinos have already been detected. Another guaranteed although not yet detected flux is that of neutrinos generated in collisions of ultra-energetic protons with the 3K cosmic microwave background (CMB), the so-called GZK (Greisen-Zatsepin-Kuzmin) neutrinos. Whereas there is a good chance that GZK and AGN neutrinos will be detected in the next decade, no practicable idea exists how to detect 1.9 K cosmological neutrinos (the analogue to the 3K CMB). This figure is taken from the ApPEC/ASPERA Astroparticle Physics Roadmap Phase 1: “Status and Perspectives of Astroparticle Physics in Europe” (Fig.4.1) at <http://www.aspera-eu.org/images/stories/files/Roadmap.pdf>.

channels roughly equal numbers of positive, negative and neutral pions are produced. Therefore, a comparable amount of energy goes into neutrinos and the electromagnetic channel. But whereas neutrinos are only subject to redshift during propagation to Earth, electrons, positrons and γ -rays can initiate an electromagnetic cascade provided there

is a sufficient number of target photons on which the γ -rays can pair produce. In an electromagnetic cascade the original γ -ray first produces a pair on the low energy target photons where either the electron or the positron takes most of the original energy and re-creates a slightly lower energy γ -ray by inverse Compton scattering. This newly created γ -ray starts a new cycle. The cycles continue to shift the particle energies to lower values until the γ -ray energy falls below the threshold for pair production on the low energy target photons. As a consequence, the γ -ray flux piles up right below the pair production threshold with a characteristic tail extending down to lower energies. Such electromagnetic cascades can occur either within individual UHECR sources on a target of infrared and optical photons, or during propagation from the source to the observer, in which case the main target will be the CMB and, to a lesser extent, the large scale infrared background. In the latter case the Universe thus acts like a calorimeter for electromagnetic energy injected above the pair production threshold on the CMB, $\sim 10^{15}$ eV. Electromagnetic energy injected above this threshold is re-processed to a diffuse extragalactic γ -ray background at hundreds of GeV. Recently, the higher sensitivity and better angular resolution of the Fermi LAT experiment has allowed to resolve a larger fraction of this background [110] originally measured by the EGRET experiment [111]. As a consequence, the best estimate of the true diffuse extragalactic γ -ray background has decreased. This has strengthened the so called cascade bound on the diffuse cosmic neutrino flux [112] which now reads

$$(58) \quad E_\nu^2 \frac{dN_\nu}{dE_\nu} \lesssim 100 \text{ eV sr}^{-1} \text{ s}^{-1} \text{ cm}^{-2}$$

and is thus already comparable to the original Waxman-Bahcall bound Eq. (57). The cascade bound is also comparable to current experimental sensitivities [113, 114].

We now turn to one of the first scenarios for neutrino production within discrete sources: Within the “proton blazar” model, in which AGNs are hadronic accelerators, one can make a rough estimate of the diffuse neutrino flux as contributed by the cosmological distribution of all proton blazars as follows [115]:

- The size of the accelerator is $R \sim \Gamma T$, where the jet boost factor is $\Gamma \sim 10$ and the duration of observed bursts is $T \sim 1$ day.
- The magnetic field strength in the jet is estimated by $B^2 \sim \rho_{\text{electron}} \sim 1 \text{ erg cm}^{-3}$ from equipartition with the plasma.
- The “Hillas condition” Eq. (19) on the maximal proton energy for a relativistic shock is $E_{\text{max}} \sim eBR$ and from $p\gamma \rightarrow N\pi$ kinematics $E_{\text{max},\nu} \sim 0.1 E_{\text{max}} \sim 10^{18}$ eV.
- The neutrino luminosity is related to the γ -ray luminosity by $L_\nu \simeq \frac{3}{13} L_\gamma$ from $p\gamma \rightarrow N\pi$ kinematics.
- Assume a differential proton spectrum $\Phi_p(E) = dN_p/dE \propto E^{-2-\beta}$ and a differential γ -ray spectrum $n_\gamma(\varepsilon) = dN_\gamma/d\varepsilon \propto \varepsilon^{-2-\alpha}$. If the jet is optically thin against

$p\gamma \rightarrow N\pi$ then

$$\frac{dN_\nu}{dE_\nu} \propto \frac{dN_p}{dE}(10E_\nu) \int_{\varepsilon_{N\pi}}^{\infty} d\varepsilon \frac{dN_\gamma}{d\varepsilon} \propto E_\nu^{-2-\beta} (\varepsilon_{N\pi})^{-1-\alpha} \propto E_\nu^{-1-\beta+\alpha},$$

since the pion production threshold $\varepsilon_{N\pi} \propto E^{-1} \propto E_\nu^{-1}$.

- Combine this with the normalization,

$$\frac{dN_\nu}{dE_\nu} \simeq \frac{3}{13} \frac{L_\gamma}{E_{\max,\nu}} \frac{1-\beta+\alpha}{E_\nu} \left(\frac{E_\nu}{E_{\max,\nu}} \right)^{-\beta+\alpha}.$$

- Fold with the luminosity function of AGNs in GeV γ -rays.

The resulting diffuse energy fluence per energy decade $E_\nu^2(dN_\nu/dE_\nu)$ peaks around $E_\nu \sim 10^{17}$ eV with a maximum of $E_\nu^2(dN_\nu/dE_\nu) \simeq 10^{-6}$ GeV cm⁻² s⁻¹ sr⁻¹ [115] This optimistic model is already ruled out by the latest IceCube limits which reads $E_\nu^2(dN_\nu/dE_\nu) \lesssim 10^{-7}$ GeV cm⁻² s⁻¹ sr⁻¹ for 10^{15} eV $\lesssim E_\nu \lesssim 10^{18}$ eV [95]. Other blazar models have also been ruled out already [116].

Scenarios in which the sources of UHECR are primarily GRBs [35, 36] start to be strongly constrained by the non-observation so far of high energy neutrinos which are predicted by these scenarios, both from individual GRBs [117] and from the accumulated diffuse flux from all cosmological GRBs [37]. Since the GRB environment is sufficiently dense to confine the accelerated protons and nuclei, only neutrons produced via $p\gamma \rightarrow n\pi^+$ can contribute to the UHECR flux. This inevitably implies production of PeV scale neutrinos from the decay of the pions produced in this reaction whose fluxes have been computed in some details [118, 89]. Neutrinos can be emitted during the precursor phase, when the jet is still forming and is optically thick for electromagnetic emission, during the prompt phase when the GRB releases most of its γ -ray emission, and during the afterglow phase.

The neutrons escaping from the GRB whose β -decay back into protons which give rise to the UHECR flux $\Phi_p(E)$ per energy from the GRB. Therefore, the neutrino per energy flux from the interaction of the original accelerated proton, $p\gamma \rightarrow n\pi^+$, can be directly related to $\Phi_p(E)$ via

$$(59) \quad \Phi_\nu(E_\nu) \sim \frac{1}{\eta_\nu} \Phi_p\left(\frac{E}{\eta_\nu}\right),$$

where $\eta_\nu \simeq 0.1$ is the average neutrino energy in units of the parent proton energy. This applies as long as the pions and muons decay faster than they lose energy by interactions within the GRB. Above a certain critical energy $E_{\pi,\mu}^c$ which is typically of the order of 10^{17} eV, this is not the case any more because of the prolonged pion and muon lifetimes due to time dilation and the neutrino flux above that energy is suppressed by a factor

$\simeq E_{\pi,\mu}^c/(4E_\nu)$ compared to Eq. (59) which reflects the probability that the pion or muon decays before interacting.

The diffuse high energy neutrino flux is then obtained by folding Eq. (59) with the cosmological GRB rate and integrating over redshift. In general, the resulting flux predictions are higher than current flux limits, as has been shown for the neutrino flux associated with the prompt phase in fireball scenarios in which associated UHECR fluxes are matched with observations, for example, in Ref. [37]. This does, however, not rule out scenarios in which most of the UHECRs are produced by GRBs, because the amount of energy transferred from protons accelerated in the GRBs is uncertain by at least factors of a few.

We end with some remarks on the so called cosmogenic or GZK neutrino flux which is produced by pion production of UHECR on the CMB during propagation from the source to the observer. The flux of secondary cosmogenic neutrinos [38, 114, 119] and photons [120, 121] can in principle also probe the UHECR mass composition: Secondary γ -rays and neutrinos are essentially produced by pion production on the constituent nucleons of a nucleus with a given atomic number A , as we have seen in section 4. Therefore, if the maximal acceleration energy E_{\max} is not much larger than 10^{21} eV then for mass numbers A approaching iron group nuclei, the energy of the constituent nucleons will be below the GZK threshold for pion production on the CMB. In this case, secondary γ -ray and neutrino production can only occur by interactions with the infrared background. Compared to pion production on the CMB, the rate of pion production on the infrared background is suppressed by the relative target photon number density which is a factor of a few hundred. As a result, the cosmogenic neutrino and photon fluxes depend strongly on injection spectrum, maximal acceleration energy and mass composition. In general it will not be easy to break the resulting degeneracies.

* * *

This work was supported by the Deutsche Forschungsgemeinschaft through the collaborative research centre SFB 676 Particles, Strings and the Early Universe: The Structure of Matter and Space-Time and by the State of Hamburg, through the Collaborative Research program Connecting Particles with the Cosmos within the framework of the Landesexzellenzinitiative (LEXI).

REFERENCES

- [1] V. F. Hess, Phys. Z. **13** (1912) 1084.
- [2] P. Auger, R. Maze, T. Grivet-Meyer, *Académie des Sciences* **206** (1938) 1721; P. Auger, R. Maze, *ibid.* **207** (1938) 228.
- [3] for a recent introduction to cosmic rays see, e.g., T. Stanev, *High Energy Cosmic Rays* (Springer 2004).
- [4] see, e.g., S. P. Swordy et al., *Astrophys. J.* **330** (1990) 625.
- [5] V. S. Berezhinsky, S. V. Bulanov, V. A. Dogiel, V. L. Ginzburg, and V. S. Ptuskin (1990), *Astrophysics of Cosmic Rays*, North-Holland, Amsterdam.
- [6] J. R. Hoerandel, *Astropart. Phys.* **21**, 241 (2004) [arXiv:astro-ph/0402356].

- [7] R. Aloisio, V. Berezhinsky, P. Blasi, A. Gazizov, S. Grigorieva and B. Hnatyk, arXiv:astro-ph/0608219; and references therein.
- [8] M. Lemoine, Phys. Rev. D **71**, 083007 (2005) [arXiv:astro-ph/0411173].
- [9] G. Sigl and E. Armengaud, JCAP **0510**, 016 (2005) [arXiv:astro-ph/0507656].
- [10] A. A. Watson, Nucl. Phys. Proc. Suppl. **151**, 83 (2006) [arXiv:astro-ph/0410514].
- [11] R. U. Abbasi *et al.* [The High Resolution Fly's Eye Collaboration], Astrophys. J. **622**, 910 (2005) [arXiv:astro-ph/0407622].
- [12] T. Abu-Zayyad *et al.* [HiRes-MIA Collaboration], Astrophys. J. **557**, 686 (2001) [arXiv:astro-ph/0010652].
- [13] J. Linsley, Phys. Rev. Lett. **10**, 146 (1963).
- [14] D. J. Bird *et al.*, Astrophys. J. **441**, 144 (1995).
- [15] J. W. Elbert and P. Sommers, Astrophys. J. **441**, 151 (1995) [arXiv:astro-ph/9410069].
- [16] N. Hayashida *et al.*, Phys. Rev. Lett. **73**, 3491 (1994); S. Yoshida *et al.*, Astropart. Phys. **3**, 105 (1995); M. Takeda *et al.*, Phys. Rev. Lett. **81**, 1163 (1998) [arXiv:astro-ph/9807193].
- [17] K. Greisen, Phys. Rev. Lett. **16**, 748 (1966); G. T. Zatsepin and V. A. Kuzmin, JETP Lett. **4**, 78 (1966) [Pisma Zh. Eksp. Teor. Fiz. **4**, 114 (1966)].
- [18] F. W. Stecker, Phys. Rev. Lett. **21**, 1016 (1968).
- [19] D. Harari, S. Mollerach, E. Roulet, JCAP **0611**, 012 (2006). [astro-ph/0609294].
- [20] D. Allard, N. G. Busca, G. Decerprit, A. V. Olinto and E. Parizot, JCAP **0810**, 033 (2008) [arXiv:0805.4779 [astro-ph]].
- [21] R. Abbasi *et al.* [HiRes Collaboration], Phys. Rev. Lett. **100**, 101101 (2008) [arXiv:astro-ph/0703099]; R. U. Abbasi *et al.*, Astropart. Phys. **32**, 53 (2009) [arXiv:0904.4500 [astro-ph.HE]].
- [22] <http://www.cosmic-ray.org/>
- [23] J. Abraham *et al.* [Pierre Auger Collaboration], Phys. Rev. Lett. **101**, 061101 (2008) [arXiv:0806.4302 [astro-ph]]; J. Abraham *et al.* [The Pierre Auger Collaboration], Phys. Lett. B **685**, 239 (2010) [arXiv:1002.1975 [astro-ph.HE]].
- [24] F. Salamida *et al.* [The Pierre Auger Collaboration], [arXiv:1107.4809].
- [25] <http://www.auger.org/>; for more details on data, see http://www.auger.org/technical_info/icrc_2011.html.
- [26] A. Castellina, F. Donato, [arXiv:1110.2981 [astro-ph.GA]].
- [27] A. Letessier-Selvon, T. Stanev, Rev. Mod. Phys. **83**, 907-942 (2011). [arXiv:1103.0031 [astro-ph.HE]].
- [28] E. Fermi, Phys. Rev. **75**, 1169-1174 (1949).
- [29] R. Blandford, D. Eichler, Phys. Rept. **154**, 1-75 (1987).
- [30] A. M. Hillas, Ann. Rev. Astron. Astrophys. **22** (1984) 425.
- [31] R. V. E. Lovelace, Nature **262**, 649 (1976).
- [32] R. D. Blandford, Phys. Scripta **T85**, 191 (2000) [arXiv:astro-ph/9906026].
- [33] K. Ptitsyna and S. Troitsky, arXiv:0808.0367 [astro-ph].
- [34] M. V. Medvedev, Phys. Rev. E **67**, 045401 (2003) [arXiv:astro-ph/0303271].
- [35] E. Waxman, Phys. Rev. Lett. **75**, 386-389 (1995). [astro-ph/9505082].
- [36] see, e.g., C. D. Dermer, arXiv:1008.0854 [astro-ph.HE].
- [37] M. Ahlers, M. C. Gonzalez-Garcia, F. Halzen, Astropart. Phys. **35**, 87-94 (2011). [arXiv:1103.3421 [astro-ph.HE]].
- [38] L. A. Anchordoqui, H. Goldberg, D. Hooper, S. Sarkar and A. M. Taylor, Phys. Rev. D **76**, 123008 (2007) [arXiv:0709.0734 [astro-ph]].
- [39] D. Eichler, D. Guetta and M. Pohl, Astrophys. J. **722**, 543 (2010) [arXiv:1007.3742 [astro-ph.HE]].
- [40] <http://icecube.wisc.edu/>

- [41] S. Toscano [IceCube Collaboration], Nucl. Phys. Proc. Suppl. **212-213**, 201 (2011) [arXiv:1105.2326 [astro-ph.HE]].
- [42] M. Aglietta *et al.* [EAS-TOP collaboration], Astrophys. J. Lett. **692**, L130 (2009) [arXiv:0901.2740v1 [astro-ph.HE]].
- [43] R. Abbasi *et al.* [IceCube Collaboration], arXiv:1109.1017 [hep-ex].
- [44] J. Abraham *et al.* [Pierre Auger Collaboration], Science **318**, 938 (2007) [arXiv:0711.2256 [astro-ph]]; J. Abraham *et al.* [Pierre Auger Collaboration], Astropart. Phys. **29**, 188 (2008) [Erratum-ibid. **30**, 45 (2008)] [arXiv:0712.2843 [astro-ph]].
- [45] P. Abreu *et al.* [Pierre Auger Observatory Collaboration], Astropart. Phys. **34**, 314 (2010) [arXiv:1009.1855 [astro-ph.HE]].
- [46] R. U. Abbasi *et al.*, Astropart. Phys. **30**, 175 (2008) [arXiv:0804.0382 [astro-ph]].
- [47] G. B. Thomson, PoS **ICHEP2010**, 448 (2010) [arXiv:1010.5528 [astro-ph.HE]].
- [48] M. J. Hardcastle, MNRAS **405**, 2810 (2010) [arXiv:1003.2500 [astro-ph.HE]].
- [49] D. Gorbunov, P. Tinyakov, I. Tkachev *et al.*, JETP Lett. **87**, 461-463 (2008). [arXiv:0711.4060 [astro-ph]].
- [50] see, e.g., F. M. Rieger, F. A. Aharonian, [arXiv:0910.2327 [astro-ph.HE]].
- [51] Fermi LAT Collaboration, Science **328**, 725 (2010) [arXiv:1006.3986 [astro-ph.HE]].
- [52] A. Falcone, H. Hase, C. Pagoni and C. Ploetz [Fermi Collaboration], Astrophys. J. **719**, 1433 (2010) [arXiv:1006.5463 [astro-ph.HE]].
- [53] M. Kachelriess, S. Ostapchenko and R. Tomas, New J. Phys. **11**, 065017 (2009) [arXiv:0805.2608 [astro-ph]]; M. Kachelriess, S. Ostapchenko and R. Tomas, arXiv:1002.4874 [astro-ph.HE].
- [54] F. Aharonian *et al.*, Astrophys. J. Lett. **695**, L40 (2009)
- [55] E. S. Seo and V. S. Ptuskin, Astrophys. J. **431**, 705 (1994).
- [56] <http://galprop.stanford.edu/>
- [57] <http://www.desy.de/maccione/DRAGON/index.html>
- [58] G. Di Bernardo, C. Evoli, D. Gaggero, D. Grasso, L. Maccione, Astropart. Phys. **34**, 274-283 (2010). [arXiv:0909.4548 [astro-ph.HE]].
- [59] see, for example, G. Morlino, D. Caprioli, [arXiv:1105.6342 [astro-ph.HE]].
- [60] F. Aharonian, A. Bykov, E. Parizot, V. Ptuskin, A. Watson, [arXiv:1105.0131 [astro-ph.HE]].
- [61] M. S. Longair and R. A. Sunyaev, Sov. Phys. Usp. **14** (1972) 569; M. T. Ressel and M. S. Turner, Comments Astrophys. **14** (1990) 323.
- [62] J. L. Puget, F. W. Stecker, and J. H. Bredekamp, Astrophys. J. **205** (1976) 638.
- [63] G. R. Blumenthal, Phys. Rev. D **1**, 1596 (1970).
- [64] M. J. Chodorowski, A. A. Zdziarski, M. Sikora, Astrophys. J. **400**, 181 (1992).
- [65] A. Mucke, R. Engel, J. P. Rachen, R. J. Protheroe and T. Stanev, Comput. Phys. Commun. **124**, 290 (2000)
- [66] E. Khan, S. Goriely, D. Allard, E. Parizot, T. Suomijarvi, A. J. Koning, S. Hilaire, M. C. Duijvestijn, Astropart. Phys. **23**, 191-201 (2005). [astro-ph/0412109].
- [67] E. Waxman, J. Miralda-Escude, Astrophys. J. **472**, L89-L92 (1996). [astro-ph/9607059].
- [68] G. Giacinti, M. Kachelriess, D. V. Semikoz and G. Sigl, arXiv:1006.5416 [astro-ph.HE]; G. Giacinti, M. Kachelriess, D. V. Semikoz, G. Sigl, Astropart. Phys. **35**, 192-200 (2011). [arXiv:1104.1141 [astro-ph.HE]].
- [69] P. P. Kronberg, Rept. Prog. Phys. **57**, 325-382 (1994); J. P. Vallee, Fundamentals of Cosmic Physics **19**, 1 (1997).
- [70] P. Blasi, S. Burles, A. V. Olinto, Astrophys. J. **514**, L79-L82 (1999). [astro-ph/9812487].
- [71] Y. Xu, P. P. Kronberg, S. Habib *et al.*, Astrophys. J. **637**, 19-26 (2006). [astro-ph/0509826].
- [72] D. Grasso, H. R. Rubinstein, Phys. Rept. **348**, 163-266 (2001). [astro-ph/0009061].
- [73] A. Neronov, I. Vovk, Science **328**, 73 (2010). [arXiv:1006.3504 [astro-ph.HE]].

- [74] K. Dolag, D. Grasso, V. Springel and I. Tkachev, JETP Lett. **79**, 583 (2004) [Pisma Zh. Eksp. Teor. Fiz. **79**, 719 (2004)] [arXiv:astro-ph/0310902]; JCAP **0501**, 009 (2005) [arXiv:astro-ph/0410419].
- [75] G. Sigl, F. Miniati and T. A. Enßlin, Phys. Rev. D **70**, 043007 (2004) [arXiv:astro-ph/0401084];
- [76] S. Das, H. Kang, D. Ryu and J. Cho, Astrophys. J. **682**, 29 (2008) arXiv:0801.0371 [astro-ph]; D. Ryu, S. Das and H. Kang, Astrophys. J. **710**, 1422 (2010) [arXiv:0910.3361 [astro-ph.HE]].
- [77] D. Ryu, H. Kang, and P. L. Biermann, Astron. Astrophys. **335** (1998) 19.
- [78] F. Miniati, “Inter-galactic Shock Acceleration and the Cosmic Gamma-ray Background,” Mon. Not. Roy. Astron. Soc. **337**, 199 (2002) [arXiv:astro-ph/0203014].
- [79] G. Sigl, F. Miniati and T. Ensslin, Nucl. Phys. Proc. Suppl. **136**, 224 (2004) [arXiv:astro-ph/0409098].
- [80] T. Stanev, R. Engel, A. Mucke, R. J. Protheroe, J. P. Rachen, Phys. Rev. **D62**, 093005 (2000). [astro-ph/0003484].
- [81] N. Globus, D. Allard, E. Parizot, [arXiv:0709.1541 [astro-ph]].
- [82] E. Armengaud, G. Sigl, T. Beau, F. Miniati, Astropart. Phys. **28**, 463-471 (2007). [astro-ph/0603675].
- [83] <http://apcauger.in2p3.fr/CRPropa/index.php> and <https://crpropa.desy.de/>
- [84] J. Abraham *et al.* [Pierre Auger Observatory Collaboration], Phys. Rev. Lett. **104**, 091101 (2010) [arXiv:1002.0699 [astro-ph.HE]].
- [85] P. Facal *et al.* [The Pierre Auger Collaboration], [arXiv:1107.4804].
- [86] R. U. Abbasi *et al.* [HiRes Collaboration], Phys. Rev. Lett. **104**, 161101 (2010). [arXiv:0910.4184 [astro-ph.HE]].
- [87] R. Ulrich, R. Engel, S. Muller *et al.*, [arXiv:0906.0418 [astro-ph.HE]].
- [88] J. Allen *et al.* [The Pierre Auger Collaboration], [arXiv:1107.4804].
- [89] L. A. Anchordoqui, D. Hooper, S. Sarkar and A. M. Taylor, Astropart. Phys. **29**, 1 (2008) [arXiv:astro-ph/0703001].
- [90] R. Gandhi, C. Quigg, M. H. Reno and I. Sarcevic, Phys. Rev. D **58**, 093009 (1998) [arXiv:hep-ph/9807264].
- [91] J. Abraham *et al.* [Pierre Auger Collaboration], Phys. Rev. D **79**, 102001 (2009) [arXiv:0903.3385 [astro-ph.HE]].
- [92] <http://baikalweb.jinr.ru/>
- [93] <http://antares.in2p3.fr/>
- [94] Y. Guardincerri *et al.* [The Pierre Auger Collaboration], [arXiv:1107.4805].
- [95] R. Abbasi *et al.* [IceCube Collaboration], Phys. Rev. D **83**, 092003 (2011) [arXiv:1103.4250 [astro-ph.CO]].
- [96] <http://jemeuso.riken.jp/en/index.html>
- [97] A. Kusenko, T. J. Weiler, Phys. Rev. Lett. **88**, 161101 (2002). [hep-ph/0106071].
- [98] <http://www.phys.hawaii.edu/~anita/web/index.htm>; <http://www.ps.uci.edu/~anita/>
- [99] P. W. Gorham *et al.* [The ANITA Collaboration], Phys. Rev. **D82**, 022004 (2010). [arXiv:1003.2961 [astro-ph.HE]]; P. W. Gorham *et al.*, arXiv:1011.5004 [astro-ph.HE].
- [100] S. Buitink *et al.*, arXiv:1004.0274 [astro-ph.HE].
- [101] S. ter Veen *et al.*, Phys. Rev. D **82**, 103014 (2010) [arXiv:1010.6061 [astro-ph.HE]].
- [102] <http://www.lofar.org/>
- [103] <http://www.skatelescope.org/>
- [104] P. W. Gorham, F. E. Baginski, P. Allison, K. M. Liewer, C. Miki, B. Hill, G. S. Varner, [arXiv:1102.3883 [astro-ph.IM]].

- [105] for recent reviews see, e.g., F. Halzen and D. Hooper, Rept. Prog. Phys. **65**, 1025 (2002) [arXiv:astro-ph/0204527]; A. B. McDonald, C. Spiering, S. Schonert, E. T. Kearns and T. Kajita, Rev. Sci. Instrum. **75**, 293 (2004) [arXiv:astro-ph/0311343];
- [106] U. F. Katz, C. Spiering, [arXiv:1111.0507 [astro-ph.HE]].
- [107] for recent short reviews see, e.g., H. J. Völk, Nucl. Phys. Proc. Suppl. **138**, 492 (2005) [arXiv:astro-ph/0401122]; H. J. Völk, arXiv:astro-ph/0312585.
- [108] E. Waxman and J. N. Bahcall, Phys. Rev. D **59**, 023002 (1999) [arXiv:hep-ph/9807282]; J. N. Bahcall and E. Waxman, Phys. Rev. D **64**, 023002 (2001) [arXiv:hep-ph/9902383].
- [109] K. Mannheim, R. J. Protheroe and J. P. Rachen, Phys. Rev. D **63**, 023003 (2001) [arXiv:astro-ph/9812398]; J. P. Rachen, R. J. Protheroe and K. Mannheim, arXiv:astro-ph/9908031.
- [110] A. A. Abdo *et al.* [The Fermi-LAT Collaboration], Phys. Rev. Lett. **104**, 101101 (2010). [arXiv:1002.3603 [astro-ph.HE]].
- [111] A. W. Strong, I. V. Moskalenko, O. Reimer, [astro-ph/0306345].
- [112] V. S. Berezinsky, A. Y. Smirnov, Astrophys. Space Sci. **32**, 461-482 (1975).
- [113] V. Berezinsky, A. Gazizov, M. Kachelriess *et al.*, [arXiv:1003.1496 [astro-ph.HE]].
- [114] M. Ahlers, L. A. Anchordoqui, M. C. Gonzalez-Garcia *et al.*, Astropart. Phys. **34**, 106-115 (2010). [arXiv:1005.2620 [astro-ph.HE]].
- [115] F. Halzen, E. Zas, Astrophys. J. **488**, 669-674 (1997). [astro-ph/9702193].
- [116] F. W. Stecker, Phys. Rev. **D72**, 107301 (2005). [astro-ph/0510537].
- [117] R. Abbasi *et al.* [IceCube Collaboration], Phys. Rev. Lett. **106**, 141101 (2011). [arXiv:1101.1448 [astro-ph.HE]].
- [118] E. Waxman, J. N. Bahcall, Phys. Rev. Lett. **78**, 2292-2295 (1997). [astro-ph/9701231].
- [119] K. Kotera, D. Allard, A. V. Olinto, [arXiv:1009.1382 [astro-ph.HE]].
- [120] G. B. Gelmini, O. E. Kalashev and D. V. Semikoz, JCAP **0711**, 002 (2007) [arXiv:0706.2181 [astro-ph]].
- [121] D. Hooper, A. M. Taylor and S. Sarkar, arXiv:1007.1306 [astro-ph.HE].

